LONG-TERM PERSPECTIVES ON NORTHERN ROCKIES CLIMATIC VARIABILITY FROM TREE RINGS IN GLACIER NATIONAL PARK, MONTANA

by

Gregory Thomas Pederson

A thesis submitted in partial fulfillment
of the requirements for the degree

of

Master of Science

in

Land Resources and Environmental Science

MONTANA STATE UNIVERSITY
Bozeman, Montana

April 2004

APPROVAL

of a thesis submitted by

Gregory Thomas Pederson

This thesis has been read by each member of the thesis committee and has been found to be satisfactory regarding content, English usage, format, citations, bibliographic style, and consistency, and is ready for submission to the College of Graduate Studies.

Dr. Lisa J. Graumlich

Approved for the Department of Land Resources and Environmental Science

Dr. Jon M. Wraith

Approved for the College of Graduate Studies

Dr. Bruce McLeod

STATEMENT OF PERMISSION TO USE

In presenting this thesis in partial fulfillment of the requirements for a master's degree at Montana State University, I agree that the Library shall make it available to borrowers under rules of the Library.

If I have indicated my intention to copyright this thesis by including a copyright notice page, copying is allowable only for scholarly purposes, consistent with "fair use" as prescribed in the U.S. Copyright Law. Requests for permission for extended quotation from or reproduction of this thesis in whole or in parts may be granted only by the copyright holder.

Gregory Thomas Pederson
April 19, 2004

ACKNOWLEDGEMENTS

I extend special thanks for the time investment, project guidance and financial support provided by Dr. Lisa J. Graumlich and Dr. Daniel B. Fagre. The quality of the research and thesis was substantially improved through comments from Dr. Stephen T. Gray and my committee members Dr. William W. Locke and Dr. Brian L. McGlynn. Jeremy Littell, Brian Peters and Blase Reardon provided hours of research discussion and field assistance; without their help this project would not have been possible. I thank Anne Schrag for editing the thesis and additional support. Andy Bunn, Karen Holzer, Todd Kipfer, Lisa McKeon, Dave Selkowitz, Andra Toivola, and Lindsey Waggoner provided technical assistance, data, and additional hands in the field. Finally, I thank Brian Luckman, Emma Watson, Roseanne D'Arrigo, and data contributors to the World Data Center for Paleoclimatology at NOAA for sharing their climate and sea surface temperature reconstructions. This work was funded by United States Geological Survey and would not have been possible without permission from Glacier National Park.

TABLE OF CONTENTS

TABLE OF CONTENTS CONTINUED

LIST OF TABLES

LIST OF FIGURES

Figure Page

LIST OF FIGURES CONTINUED

ABSTRACT

Instrumental climate records reveal fluctuations in summer moisture anomalies and winter snowpack in Glacier National Park, Montana, on decadal and multidecadal timescales. However, because climate records for the region are limited to the 20th century, studies on the impacts of long-duration variations in climate on physical and ecosystem processes were limited. Therefore, a reconstruction of summer moisture variability (June - August) spanning A.D. 1540-2000 was created from a multi-species network of tree-ring chronologies sampled in Glacier National Park. The reconstruction shows decadal-scale shifts between drought and pluvial events with a pronounced cool/wet period spanning the end of the Little Ice Age (A.D. 1770-1840). The single most exceptional drought event occurred over the 20th century (A.D. 1917-1941) and was associated with the most spatially consistent drought regime throughout the northern Rockies and Pacific Northwest over the past ~500 yrs. Among a wider spatial network of hydroclimatic reconstructions arrayed along a north-south Rocky Mountain transect, trends at Glacier National Park were found to be most similar to those in the Canadian Rockies and the Pacific Northwest. Also, many decadal-scale drought/pluvial events were consistent among all sites along the north-south transect - although magnitude, intensity, and time of onset varied. To investigate climatic drivers related to the Little Ice Age glacial maximum and rapid 20th-century retreat, I explored the impact of north Pacific Basin sea-surface temperature anomalies on low-frequency variations in winter snowpack for the park. Temperature anomalies in the north Pacific basin exhibit tight linkages to variations in snowpack; therefore, I used a tree-ring based reconstruction of north Pacific temperature variability and summer drought as proxies for winter glacial accumulation and summer ablation, respectively, over the past three centuries (A.D. 1700-2000). These records show that the 1850's glacial maximum was likely produced by ~70 yrs of cool/wet summers coupled with high snowpack. Glacial retreat coincided with an extended period (>50 yr) of summer drought and low snowpack culminating in the exceptional events of 1917-1941 when retreat rates exceeded 100 m/yr. This research highlights the difficulty in detecting regional expression of global climate change when 'natural' decadal-scale variations in climate are regionally common.

CHAPTER 1

THESIS OVERVIEW

Introduction

Evidence of twentieth-century glacial recession in Glacier National Park (GNP), Montana, indicates that climatic warming over the past century has been substantial. Glaciers integrate differences in temperature and precipitation across regions, thus serving as regional indicators of climatic change. Within the park, glaciers were at their late-neoglacial maximum during the mid–nineteenth century in a time period known as the Little Ice Age (LIA; ~ 14^{th} to 19^{th} century A.D. [Carrara and McGimsey, 1981]). At the height of the LIA, 150 glaciers and perennial snow/ice fields located within the park covered approximately 99 km^2; currently, less than 40 glaciers and ice fields exist, covering an area less than 26 km^2 (Key et al., 2002). In light of the rapid glacial retreat within the park, and predictions made by Hall and Fagre (2003) indicating complete ablation of glaciers within the park by 2030, establishing the pattern of climatic variability that drives the observed glacial dynamics has become a priority. This knowledge may aid in an assessment of the degree to which the observed late 20^{th}-century trends in climate and glacial recession fall outside the natural range of variability (if at all). Portions of the headwater regions of the Canadian South Saskatchewan and the U.S. Columbia and Missouri river systems are contained within GNP, thus making the park a key area of hydrologic output during spring runoff and summer base-flow periods. In order to evaluate the future implications of glacial dynamics on ecosystem processes

and natural resources, an understanding of decadal and multidecadal drivers of regional climate is needed.

Drivers of Climate Variability in GNP

GNP is located in a region strongly affected by ocean-atmosphere climate interactions, including the Southern Oscillation and the Pacific Decadal Oscillation (PDO; see Mantua and Hare [2002]). Persistent ocean-atmosphere anomalies, such as PDO, have the potential to generate long-duration (decadal and longer) patterns of change in precipitation and temperature. PDO fluctuations include warm (positive) phases and cool (negative) phases in ocean-surface temperatures approximately every 20 to 30 years, which correspond to warmer and drier or cooler and wetter conditions respectively throughout the Pacific Northwest (Biondi et al., 2001). The El Niño Southern Oscillation (ENSO) also fluctuates between a warm (positive) phase (El Niño) and cool (negative) phase (La Niña), each lasting 6 to 18 months (Hare and Mantua, 2001). The primary region influenced by PDO is the Pacific Northwest whereas ENSO tends to dominate the Southwestern regions of North America and the tropics (Mantua and Hare, 2001). Due to the strong Pacific Maritime influence on GNP, the PDO may have a stronger role than ENSO in driving low-frequency climatic variability.

Climate Variation and Glacial Dynamics

Climate variation influences glacial fluctuations through synoptic patterns in atmospheric circulation, long-term trends in temperature and precipitation patterns, and local topography. Throughout the Pacific Northwest, including Washington, Alaska,

western Canada, and the southern Cascades, glaciers have been shown to respond to climatic change on decade to century time scales through low-frequency synoptic patterns linked-in-part to PDO (e.g. Yarnal, 1984; Changnon et al., 1993; McCabe and Fountain, 1995; Hodge et al., 1998; and Bitz and Battisti, 1999). Yarnal (1984) investigated the relationship between mass balance of glaciers in southwestern Canada and 500mbar atmospheric patterns and demonstrated the types of synoptic patterns (cyclonic or anticyclonic, and small- or large-scale) that favored glacial accumulation and ablation. In a related study, Changnon (1993) observed long-term wet and dry periods in snowpack along a north to south gradient of the northern U.S. Rocky Mountains and its association with 500mbar synoptic patterns.

Other studies have highlighted the importance of temporal variation in temperature and precipitation on glacial fluctuations. Regionally, a study by Bitz and Battisti (1999) linked impacts of long-term temporal variability on fluctuations in glacial mass balance resulting from a "decadal ENSO-like climate phenomena", which explained up to 35% of the net winter mass balance in maritime glaciers along the western coast of North America. Interestingly, the ENSO-like phenomena later became better known as PDO. Bitz and Battisti (1999) also state that ENSO was only weakly related to the mass balance of these glaciers because precipitation anomalies associated with ENSO lie far to the south. More recent studies connect fluctuations (over 20 to 30 yrs) in spring snowpack within GNP (Selkowitz et al., 2002) and for the entire western U.S. (McCabe and Dettinger, 2002) to PDO, which therefore, creates fluctuations in winter glacial accumulation with obvious implications for annual mass balance.

Over the summer season, decadal variability in precipitation (i.e. moisture anomalies or drought) throughout the western U.S. exhibits ocean-based linkages similar to the PDO that extend primarily from the tropical Pacific (Cayan et al., 1998). Such relationships, however, tend to be reduced in strength compared with those observed over the winter season. Other recent evidence indicates that summer hydroclimatic variability may be controlled in spatial extent and temporal duration through phase coupling between the north Pacific basin and the north Atlantic via PDO and the Atlantic Multidecadal Oscillation (AMO; see Enfield et al. [2001]; and McCabe and Palecki [2004]). Although the action centers related to summer and winter precipitation patterns originate in different regions of the Pacific and Atlantic, precipitation during both seasons has been shown to fluctuate on decadal and longer scales. However, each of the aforementioned studies utilized instrumental records that are hindered by their short duration; consequently limiting the analysis to the 20th century. As a result, it's difficult to capture the full range of 'natural' climate variability in both the low- and high-frequency domains.

Climate Variability from Tree Rings

Throughout North America tree rings have been widely used as proxies for instrumental climate often providing a continuous record spanning centuries to millennia, and yielding high-resolution data that is particularly well suited for capturing interannual and decadal-scale (>10 yr) variations in climate (Fritts, 1976; Cook and Kairiukstis, 1990). In the western U.S. and Pacific Northwest there have been many climate reconstructions from tree rings that have shed light on decadal- to century-scale climatic

variation on local to regional scales. For example, in Canada moisture anomaly reconstructions exist for the Rocky Mountain foothills and the eastern high plains (Case and MacDonald, 1995; and Sauchyn and Beaudoin, 1998). Throughout the Canadian Cordillera and U.S. northern Rockies a network of reconstructions for annual precipitation and summer temperatures has been completed (e.g. Luckman et al., 1997; St. George and Luckman, 2001; Watson and Luckman 2001; Wilson and Luckman, 2003). For the U.S., Yellowstone National Park, Wyoming (Gray et al., 2003), the central United States (Woodhouse and Overpeck, 1998), the Unita Basin in Utah (Gray et al., 2004), and the Pacific Northwest (Graumlich and Brubaker, 1986; Graumlich, 1987; Garfin and Hughes, 1996) extensive reconstructions have been accomplished for precipitation and temperature. Prior to this study, however, the northern U.S. Rocky Mountains lacked tree-ring based reconstructions of climate, thus inhibiting development of knowledge related to local and regional drivers of drought and glacial dynamics.

Within the northern and southern Canadian Rockies, dendroglaciology and paleoclimatic reconstructions from tree rings, have demonstrated decadal-scale responses in glacial dynamics to regional climatic variability. Here, Luckman (1993; 2000) identifies long-duration drivers of glacial dynamics by demonstrating synchronous events related to variations in climate in both tree rings and glaciers. By using tree-ring reconstructions of temperature and precipitation, Luckman (1993; 2000) correlated glacial retreat with periods of higher than average summer temperature and lower annual precipitation. Thus, Luckman (2000) concludes that the LIA was not the sole result of a multi-centennial simple cooling trend of the Northern Hemisphere; rather, the climate

over the last millennium demonstrates variability dominated by decade-century patterns. Though Luckman points out specifics in the Canadian Rockies, the LIA was a globally expressed phenomenon.

Thesis Objectives

Studies of the western U.S. and Canada using instrumental and proxy climate data indicate the prevalence of decadal and multidecadal shifts or 'regimes' throughout the region. Understanding these low-frequency variations in climate is a necessary first step in discovering regional impacts extending from anthropogenic warming, and management of natural resources - especially water. Therefore the primary objective of my work was to develop a multi-species network of tree-ring data for investigation of long-term trends and fluctuations in climate for the GNP region. Consequently, I produced a summer moisture anomaly reconstruction spanning the past 461 yrs, and describe the nature of the decadal-scale variability contained within. Also, I sought to link hydroclimatic variability in the Glacier National Park region to a wider network of precipitation reconstructions throughout western North America. The final goal of my research was to synthesize multiple lines of paleo-proxy data related to the physical drivers of glacial dynamics to produce a coherent picture (or theory) of processes resulting in the LIA glacial maximum and subsequent rapid 20th century retreat.

The following two chapters were arranged such that chapter 2 constructs the foundation of the paleoclimatic data that is further analyzed in chapter 3 for linkages with glacial dynamics. In chapter 2, I describe methods for constructing Douglas-fir and limber pine ring-width chronologies for the region. Then, I provide a reconstruction of

summer moisture anomalies spanning 461 yrs (A.D. 1540-2000) based upon a subset of the most sensitive ring-width chronologies from the network. Both wet and dry events over the summer season are then classified in terms of intensity, magnitude and duration for all decadal-scale events. Comparisons are then made between the instrumental and reconstructed periods. To conclude, reconstructed drought and pluvial events in Glacier National Park are compared to other moisture-sensitive reconstructions along a north to south Rocky Mountain transect spanning the U.S. and Canada.

Chapter 3 builds on the summer moisture anomaly reconstructions for the park by synthesizing data and research related to winter snowpack and glacial dynamics for the region. I therefore provide a perspective on physical processes leading up to the LIA glacial maximum and subsequent 20th century retreat along with a baseline measure of 'normal' climatic variations for the region. The importance of this study is not limited to the investigation of climate change within the park. Rather, it provides a paleoclimatic background of events upon which other research studies related to ecosystem processes and global climate change may rely, along with critical information for use in the management of natural resources for the park and adjacent regions.

REFERENCES CITED

Biondi, F., Gershunov, A., Cayan, D.R., 2001. North Pacific decadal climate variability since 1661. *Journal of Climate* 14, 5-10.

Bitz, C.M., Battisti, D.S., 1999. Interannual to decadal variability in climate and glacier mass balance in Washington, Western Canada, and Alaska. *Journal of Climatology* 12, 3181-3196.

Carrara, P.E., McGimsey, R.G., 1981. The late-neoglacial histories of the Agassiz and Jackson Glaciers, Glacier National Park, Montana. *Arctic and Alpine Research* 13(2), 183-196.

Case, R.A., MacDonald, G.M., 1995. A dendroclimatic reconstruction of annual precipitation on the western Canadian prairies, since A.D. 1505 from *Pinus flexilis* James. *Quaternary Research* 44, 267-275.

Cayan, D.R., Dittinger, M.D., Diaz, H.F., Graham, N., 1998. Decadal variability of precipitation over western North America. *Journal of Climatology* 11, 3148-3166.

Changnon, D., McKee, T.B., Doesken, N.J., 1993. Annual snowpack patterns across the Rockies: Long-term trends and associated 500-mb synoptic patterns. *Monthly Weather Review* 121, 633-647.

Cook, E.R., Kairiukstis, L., 1991. *Methods of Dendrochronology: Applications in the Environmental Sciences.* Kluwer Academic Publishers, Dordrecht.

Enfield, D.B., Mestas-Nunez, A.M., Trimble, P.J., 2001. The Atlantic multidecadal oscillation and its relation to rainfall and river flows in the continental U.S. *Geophysical Research Letters* 28(10), 2077-2080.

Fritts, H.C., 1976. *Tree Rings and Climate*. Academic Press, New York.

Garfin, G.M., Hughes, M.K., 1996. Eastern Oregon divisional precipitation and Palmer Drought Severity Index from tree-rings. *Report to the U.S. Forest Service Intermountain Research Station*.

Graumlich, L.J., 1987. Precipitation variation in the Pacific Northwest (1675-1975) as reconstructed from tree rings. *Annals of the Association of American Geographers* 77, 19-29.

Graumlich, L.J., Brubaker, L.B., 1986. Reconstruction of annual temperature (1590-1979) for Longmire, Washington, derived from tree rings. *Quaternary Research* 25, 223-234.

Gray, S.T., Betancourt, J.L., Fastie, C.L., Jackson, S.T., 2003. Patterns and sources of multidecadal oscillations in drought-sensitive tree-ring records from the central and southern Rocky Mountains. *Geophysical Research Letters* 30(6), doi:10.1029/2002GL016154.

Gray, S.T., Jackson, S.T., Betancourt, J.L., 2004. Tree-ring based reconstructions of interannual to decadal precipitation variability for northeastern Utah. *Journal of American Water Resources*, in press.

Hall, M.P., Fagre, D.B., 2003. Modeled climate-induced glacier change in Glacier National Park, 1850-2100. *BioScience* 53(2), 131-140.

Hare, S.R, Mantua, N.J., 2001. An historical narrative on the Pacific Decadal Oscillation, interdecadal climate variability, and ecosystem impacts. *20th NE Pacific Pink and Chum Workshop.* Seattle, WA.

Hodge, S.M., Trabant, D.C., Krimmel, R.M., Heinrichs, T.A., March, R.S., Josberger, E.G., 1998. Climate variations and changes in mass of three glaciers in Western North America. *Journal of Climate* 11, 2161-2179.

Key, C.H., Fagre, D.B., Menicke, R.K., 2002. Glacier retreat in Glacier National Park, Montana. *Satellite Image Atlas of Glaciers of the World*. pp. J1- J12.

Luckman, B.H., 1993. Glacier fluctuation and tree-ring records for the last millennium in the Canadian Rockies. *Quaternary Science Review* 12, 441-450.

Luckman, B.H., Briffa, K.R., Jones, P.D., Schweingruber, F.H., 1997. Summer temperatures at the Columbia Icefield, Alberta, Canada, 1073-1987. *The Holocene* 7, 375-389.

Luckman, B.H., 2000. The Little Ice Age in the Canadian Rockies. *Geomorphology* 32, 357-384.

Mantua, N.J., Hare, S.R., 2002. The Pacific Decadal Oscillation. *Journal of Oceanography* 58, 35-44.

McCabe, G.J., Dettinger, M.D., 2002. Primary modes and predictability of year-to-year snowpack variations in the western United States from teleconnections with Pacific Ocean climate, *Journal of Hydrometeorology* 3, 13-25.

McCabe, G.J., Fountain, A.G., 1995. Relations between atmospheric circulation and mass balance of South Cascade Glacier, Washington, U.S.A., *Arctic and Alpine Research* 27(3), 226-233.

McCabe, G.J., Palecki, M.A., Betancourt, J.L. 2004. Pacific and Atlantic Ocean influences on multidecadal drought frequency in the United States. *Proceedings of the National Academy of Sciences,* In press.

Sauchyn, D.J., Beaudoin, A.B., 1998. Recent environmental change in the southwestern Canadian Plains. *The Canadian Geographer* 42, 337-353.

Selkowitz, D.J., Fagre, D.B., Reardon, B.A., 2002. Interannual variations in snowpack in the crown of the continent ecosystem. *Hydrological Processes* 16, 3651-3665.

St. George, S., Luckman, B.H., 2001. Extracting a paleotemperature record from *Pica englmanii* treeline sites in the central Canadian Rockies. *Canadian Journal of Forest Research* 31, 457-470.

Watson, E., Luckman, B.H., 2001. Dendroclimatic reconstruction of precipitation for sites in the southern Canadian Rockies. *The Holocene* 11(2), 203-213.

Woodhouse, C.A., Overpeck, J.T., 1998. 2000 years of drought variability in the central United States. *Bulletin of the American Meteorological Society* 79, 2693-714.

Yarnal, B., 1984. Relationships between synoptic-scale atmospheric circulation and Glacier mass balance in Southwestern Canada during the international hydrological decade, 1965-74. *Journal of Glaciology* 30(105), 188-198.

CHAPTER 2

SUMMER MOISTURE VARIABILITY IN GLACIER NATIONAL PARK, MONTANA SINCE A.D. 1540

Introduction

Glacier National Park (GNP), Montana, encompasses a portion of the headwater regions for the Columbia, South Saskatchewan, and Missouri river basins (Figure 2.1). Thus, the park is a key area of hydrologic output for U.S. and Canadian river systems during spring melt and summer low-flow periods. In the recent past GNP has witnessed dramatic climate-driven events, including flooding during years 1992 and 1997, extensive wildfires during years 2000 and 2003 (over 140,000 acres burned), the lowest and highest spring snowpack levels in 34 yrs, and the continual retreat of alpine glaciers and snowfields. In order to interpret the importance of these events as either anomalous or within the range of natural variability, it is critical to place the climate of the past decades into a larger context of interannual and decadal-scale hydroclimatic variability of the U.S. northern Rocky Mountains. Instrumental climate records provide a limited context in this regard. Their short duration, rarely over 100 years, provides a limited number of decadal-scale drought and pluvial events (Cayan et al., 1998), with a high likelihood of not capturing the full range of 'baseline' variability (Woodhouse and Overpeck, 1998) - with a bias towards low elevation weather monitoring sites.

Tree rings have been widely used throughout North America as proxies for instrumental climate and have provided highly replicable information related to

interannual and decadal-scale (>10 yr) climate variability (Fritts, 1976; Cook and Kairiukstis, 1990). Regionally, dendroclimatic reconstructions have been completed for western Canada (Case and MacDonald, 1995; Luckman et al., 1997; Sauchyn and Beaudoin, 1998; St. George and Luckman, 2001; Watson and Luckman 2001; Wilson and Luckman, 2003), Yellowstone National Park, Wyoming (Gray et al., 2003), the central United States (Woodhouse and Overpeck, 1998), Utah's Unita Basin (Gray et al. 2004), and the Pacific Northwest (Graumlich and Brubaker, 1986; Garfin and Hughes, 1996). A gridded reconstruction of the Palmer Drought Severity Index (PDSI) for the United States by Cook et al. (1996; 1999) is also available; however, within this network of tree-ring reconstructions, northwestern Montana attains poor reconstruction calibration statistics potentially due to the lack of chronologies from the Rocky Mountain region.

In this paper, I present a new reconstruction of summer moisture variability (or Mean Summer Deficit [MSD]), spanning 461 years (A.D. 1540-2000), from a network of ring-width chronologies sampled in and around GNP. Decadal variations between drought and pluvial events are then classified using standard techniques, and step changes from the long-term mean (or "regime shifts") are identified using an intervention detection algorithm (Gedalof and Smith, 2001; Gray et al., 2004). After the significance of each decadal-scale regime is assessed using intervention analysis (Box and Tiao, 1975), I make objective comparisons between regimes in terms of duration, magnitude, and intensity for events in the instrumental (A.D. 1900-present) and pre-instrumental periods (A.D. 1540-1900). This allows us to place long-duration shifts in drought and pluvial events of the 20th century within the range of natural variability in light of the

previous four centuries. Finally, I compare decadal-scale moisture variability along a north to south Rocky Mountain transect encompassing Canada and the U.S.

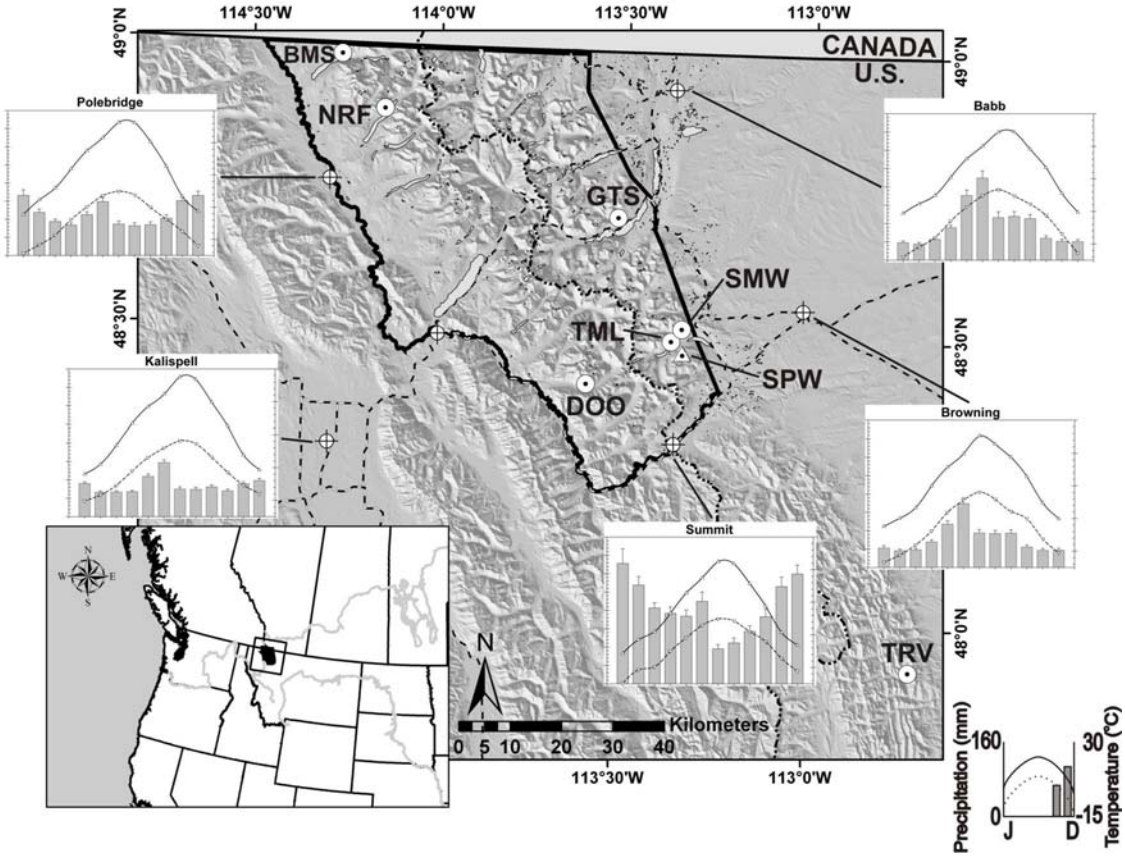

Figure 2.1. Location of tree-ring chronologies and climate stations in the Glacier National Park region. The heavy black line delineates the park boundary, and the stippled black line bisecting the park displays the path of the Continental Divide. Dotted circles and dotted triangles represent Douglas-fir and limber pine chronologies respectively. Meteorological station locations are indicated by a circle w/crosshairs and climatographs for Kalispell, Polebridge, Summit, Babb, and Browning display climate regimes of the region. Solid black lines indicate monthly mean maximum temperatures, dashed black lines display monthly mean minimum temperatures, and monthly average precipitation is graphed using gray vertical bars with error bars plotted as +1 standard error from the mean.

Study Area

Glacier National Park encompasses 4,082 km^2 of the U.S. northern Rocky Mountains and consists primarily of montane, subalpine, and alpine ecosystems. The climate of this region can be described as Pacific Maritime with Continental modifications, and is most similar climatologically, geologically and biologically to the southern Canadian Rockies (Finklin, 1986). The strong influence of the Pacific Ocean along with the orographic effects of the Continental Divide (CD), which bisects the park, causes this region to be one of the most mesic in Montana (Figure 2.1). Here, winter valley inversions are common during incursions of arctic air masses, and the annual distribution of precipitation is bimodal with significant amounts received during the early growing season (A,M,J) and over the winter months (N,D,J,F). In contrast, regions east of the Divide are strongly influenced by cold, dry continental air masses resulting in less winter precipitation and common chinook winds.

The spring influx of precipitation is common to both sides of the park, and is caused by the northward retreat of arctic cold fronts and ensuing incursion of warm moist air from the Gulf of Mexico (Cunningham, 1982). In contrast, winter precipitation is largely controlled by conditions in the north Pacific, which reflect strength and position of the Aleutian Low (McCabe and Dettinger, 2002). However, the orographic influence of the CD results in the capture of substantial proportions of precipitation by the western region and Divide ranges, while the eastern high plains receive only trace amounts over the winter months (Figure 2.1). Consequently, the majority of the park receives soil moisture recharge during winter months with typical summer drought, or moisture

deficit, resulting from high temperatures and low precipitation in July, August and September. In addition, interannual and decadal variations in snowpack (Selkowitz et al., 2002) and summer moisture anomalies (Cayan et al., 1998) appear to be common in the instrumental records for the region, indicating the potential for low-frequency seasonal climate forcings.

Data and Methods

Chronology Development

I sampled eight mid-elevation, moisture sensitive tree-ring chronologies between 2000-2002 from the Livingston, Lewis and the southeastern Teton mountain ranges (Figure 2.1; Table 2.1). The seven Douglas-fir (*Pseudotsuga menziesii* (Mirb.) Franco) chronologies and single limber pine (*Pinus flexilis* James) chronology are located east and west of the CD and arrayed along a northwest to southeast transect. Characteristics of all tree-ring sites include open-grown stands located on well-drained, relatively stable, south-facing slopes with sparse understory vegetation and little sign of recent disturbance. Soils are calcareous and originate from sedimentary rocks of the Appekunny, Prichard and Altyn Formations, which date to the Middle Proterozoic Era. The development of soil at each site is poor (depths ranging from 0-20cm) with slope angles ranging from 35-65% within each stand.

Sample collection involved double coring each tree parallel to the topographic contours of the slope approximately 1 m above ground level. Cores or cross-sections were obtained from subfossil wood for both species when available. Deadwood played

an important role in extending chronology length and adding sample depth to the early portion of the limber pine record; however, due to the high decomposition rates in Douglas-fir, subfossil wood accounts for a negligible portion of the record. A total of 243 trees (385 radii) were sampled, and chronology lengths range from 341 to 885 yrs with a minimum sample size of 12 trees and a maximum of 53 (Table 2.1). The single oldest living Douglas-fir was sampled at Spot Mountain West (SPW) and attained an age of 839 yrs. At SPW few living limber pine trees were present - the oldest of which reached 381 yrs; however, the subfossil wood produced 15 individual samples extending over 400 consecutive years, the oldest spanning 801 yrs with a termination date of A.D. 1935. Samples are property of GNP and are currently archived at the Big Sky Institute Tree-Ring Laboratory, Montana State University, Bozeman, Montana.

Table 2.1. Location and description of chronology network used in this study. Light (dark) gray shading indicates sites west (east) of the Continental Divide.

Location	Site Name	Site Code	Species[a]	Lat (ºN)	Long (ºW)	Elevation (m)	No. Trees	No. Radii	Chronology Period (yr)	SSS ≥ 0.85
West	Boundry Mountain	BMS	PSME	48° 59'	114° 15'	1710	33	64	1499 - 2002	1540(9)[b]
	Numa Ridge Falls	NRF	PSME	48° 51'	114° 12'	1695	18	34	1645 - 2001	1710(6)
	Doody Mountain	DOO	PSME	48° 23'	113° 37'	1890	20	37	1660 - 2001	1704(6)
East	Going-To-Sun	GTS	PSME	48° 42'	113° 31'	1860	12	22	1337 - 2002	1610(5)
	Two-Medicine Lake	TML	PSME	48° 29'	113° 22'	1636	34	51	1564 - 2001	1670(7)
	Spot Mountain West	SMW	PSME	48° 31'	113° 22'	1950	42	65	1163 - 2002	1386(8)
	Teton River Valley	TRV	PSME	47° 55'	112° 44'	1678	31	46	1509 - 2001	1618(8)
	Scenic Point	SPW	PIFL	48° 29'	113° 19'	2040	53	66	1115 - 2000	1268(8)
						Total:	243	385		

[a] PSME, Douglas-fir; PIFL, limber pine

[b] Number of trees

After collections were completed, cores and cross-sections were mounted, sanded and crossdated following standard techniques (Stokes and Smiley, 1968; Fritts 1976; Briffa and Jones, 1990). Measurements were made using a Velmex UniSlide traversing table and digital counter to a precision of ±0.001 mm. Accurate dating of all series was

accomplished utilizing statistical crossdating methods in the COFECHA program (Grissino-Mayer et al., 1997), and verification was achieved through comparison with nearby chronologies. Age-related growth trends in ring-width values were removed using 'conservative' detrending methods (negative exponential curve, or linear trend line of negative or zero slope), then combined into a standardized chronology using the biweight robust mean in the ARSTAN program (Cook et al., 1990). These detrending methods were selected based upon suitability of stand characteristics; consequently, they allow for the majority of the low- and high-frequency variation to be retained (Cook, 1985). In addition, the mean segment length for each chronology ranges from 220 to 376 years (mean 290), thus circumventing the "segment-length curse" (see Cook et al., 1995) and allowing for analysis of low-frequency variability.

An assessment of chronology quality, based upon the strength of common signal, was made using average correlation between series (Rbar) and the express population signal (EPS; Wigley et al., 1984). Calculations were made over a common interval (selected by ARSTAN), thus maximizing series length while retaining the greatest number of samples. All chronologies appear suitable for climatic reconstruction, obtaining EPS values ≥ 0.85 with 12 trees (on average), and for all chronologies Rbar values average 0.33 (*see* Appendix A). However, EPS does not represent the most relevant statistic of chronology error as it relates to decreasing sample depth through time. To constrain additional error in climate reconstructions resulting from decreasing sample depth in the early portion of the record, subsample signal strength (SSS; Wigley et al., 1984) was computed for each chronology. An SSS value of 0.85 was selected as

the cutoff, thus limiting the maximum amount of additional error arising from a decreasing number of trees to 15% (Table 2.1).

Climate / Ring-Width Relationships

Calibration of ring-width variability to climatic signal was conducted by running correlations between individual chronologies, local meteorological station records, and Montana state climate division data. Historical weather data was obtained from the Western Regional Climate Center (WRCC; http://www.wrcc.dri.edu/), and the U.S. Historical Climatology Network (USHCN; *see* Easterling et al., [1996]; http://cdiac.esd.ornl.gov/epubs/ndp019/ndp019.html). While all available local and regional meteorological records were used during initial stages of analysis, Kalispell was selected as the primary station for reconstruction due to length, completeness of record, and regional representation. Although the USHCN corrected temperature records for Kalispell reflect regional trends and variability, corrections made to the precipitation record are less robust. The precipitation record contains poor confidence intervals around interpolated and adjusted values, and data values were missing although the WRCC indicates a complete record. In addition, only a single year (1949) was withheld from the WRCC dataset due to a major station move and over 4 months of missing data. Therefore, I combine the USHCN temperature records with the WRCC precipitation records to produce the most serially complete climate record spanning 1900-2003 (*see* Appendix B).

Studies conducted in the surrounding region have found ring-width variability correlates strongly with annualized (e.g. Watson and Luckman, 2001; Gray et al., 2004)

or seasonal (Luckman, 1997; Wilson and Luckman, 2003) data. Thus, correlations were calculated between individual chronologies and monthly, seasonal, and annual combinations of temperature and precipitation. Also, many western U.S. chronologies integrate temperature and precipitation signals, so relationships between mean summer deficit (MSD), and the Palmer Drought Severity Index (PDSI; Palmer, 1965) were examined. Calculation of MSD (precipitation – potential evapotranspiration [Thornthwaite, 1948] for JJA) and monthly PDSI was performed using the Newhall Soil Moisture model (Newhall and Berdanier, 1996) and individual station PDSI software available from the National Agriculture Decision Support System (http://nadss.unl.edu/index.php; *see* Appendix C). Each chronology was compared against climate data at *t*, *t-1(2,3)* and *t+1(2,3)* yrs to account for lags in growth response and climatic persistence. Final selection of the climatic parameter for reconstruction was based on overall strength and significance of correlation along with the temporal stability of the climate-tree growth relationship, which was assessed using 35 yr moving correlation coefficients (MCC's) calculated using the Biondi (1997) DendroClim2002 software (*see* Appendix D). All correlation coefficients were tested for significance using a bootstrapped confidence interval by drawing and replacing 1000 random samples from the calibration period and subsequently computing the correlation coefficient for each of the respective samples (methods described in Biondi, 1997).

Identification and Detection of Decadal Climate Regimes

Initial detection of potential decadal or multi-decadal shifts in the paleo-proxy drought record involved the application of an intervention detection algorithm described by Gedalof and Smith (2001) and Gray et al. (2004). The function used was modified for the objectives of this study, and consequently designed to detect both the high- (≥6 yrs) and low-frequency (≥20 yrs) ends of a potential decadal regime (events ≥6 yrs duration are taken to be 'decadal'). The algorithm applies two-sample t-tests within multiple moving windows of length 6, 10, 16, and 20 yrs, which identify whether the mean of the first 3,5,8, and 10 yrs are significantly different from the latter. This application of multiple moving windows narrows the range of years in which a potential shift of long duration may have occurred, and provides an initial estimate of the total event duration.

Exact beginning and ending years of a regime were then identified as the first year where annual MSD values change sign for two or more consecutive years and coincide with the date the 10 yr cubic spline returns to or crosses the mean. Due to the presence of autocorrelation, assumptions of the two-sample t-test are violated resulting in an inability to determine statistical significance of each regime. Therefore, I address this potential problem using intervention analysis (Box and Tiao, 1975), whereby the first step involves the application of a univariate autoregressive integrated moving average (ARIMA; *see* Box and Jenkins [1970]) model to the MSD reconstruction. Then, each potential intervention was incorporated into a linear model as a step-change variable along with the residuals from the ARIMA model for an assessment of significance. A potential intervention with a coefficient p-value ≤0.05 was considered to be significant. Readers

seeking a more complete description of the applied approach are urged to consult Hare and Francis (1994), and Downing and McLaughlin (1990).

Each of the significant regimes identified was then classified in terms of duration, magnitude and intensity using methods outlined by Biondi et al. (2002). Duration is described here as the number of years a positive or negative intervention remains above or below the mean. Magnitude is equal to the sum of all annual MSD values for a regime over its duration, and the ratio between magnitude and duration is described as intensity. Hence, intensity is equivalent to the average magnitude of a regime, which coincidentally corresponds with the step-change value used for significance testing of each regime in intervention analysis. Finally, each regime was given a score by summing the rankings for duration, absolute magnitude, and absolute intensity. The higher an event's overall score indicates the 'stronger' the overall regime, thus allowing for a quantitative comparison between regimes in relation to the three types of descriptors.

Results

Summer Moisture Anomaly Reconstruction – Calibration and Verification

Correlation analysis for each of the eight chronologies exhibits a common relationship to monthly temperatures and precipitation (Figure 2.2*a*,*b*). The strongest monthly correlations are found between Douglas-fir ring widths and monthly mean maximum temperature (T_{max}) of the previous July (r = -0.30 - -0.63), with a consistent - but slightly reduced - response to growth year July T_{max} (r = -0.28 - -0.40). I also observe significant positive correlations (r = 0.23 - 0.49) of reduced strength (relative to T_{max}) to

previous July total precipitation (PPT). In general, the majority of the chronologies exhibit a consistent and significant response to previous growing season, or summer (J,J,A), PPT, and T_{max} with a reduced response to spring and summer conditions during the year of growth. In addition, half of the Douglas-fir chronologies respond to January

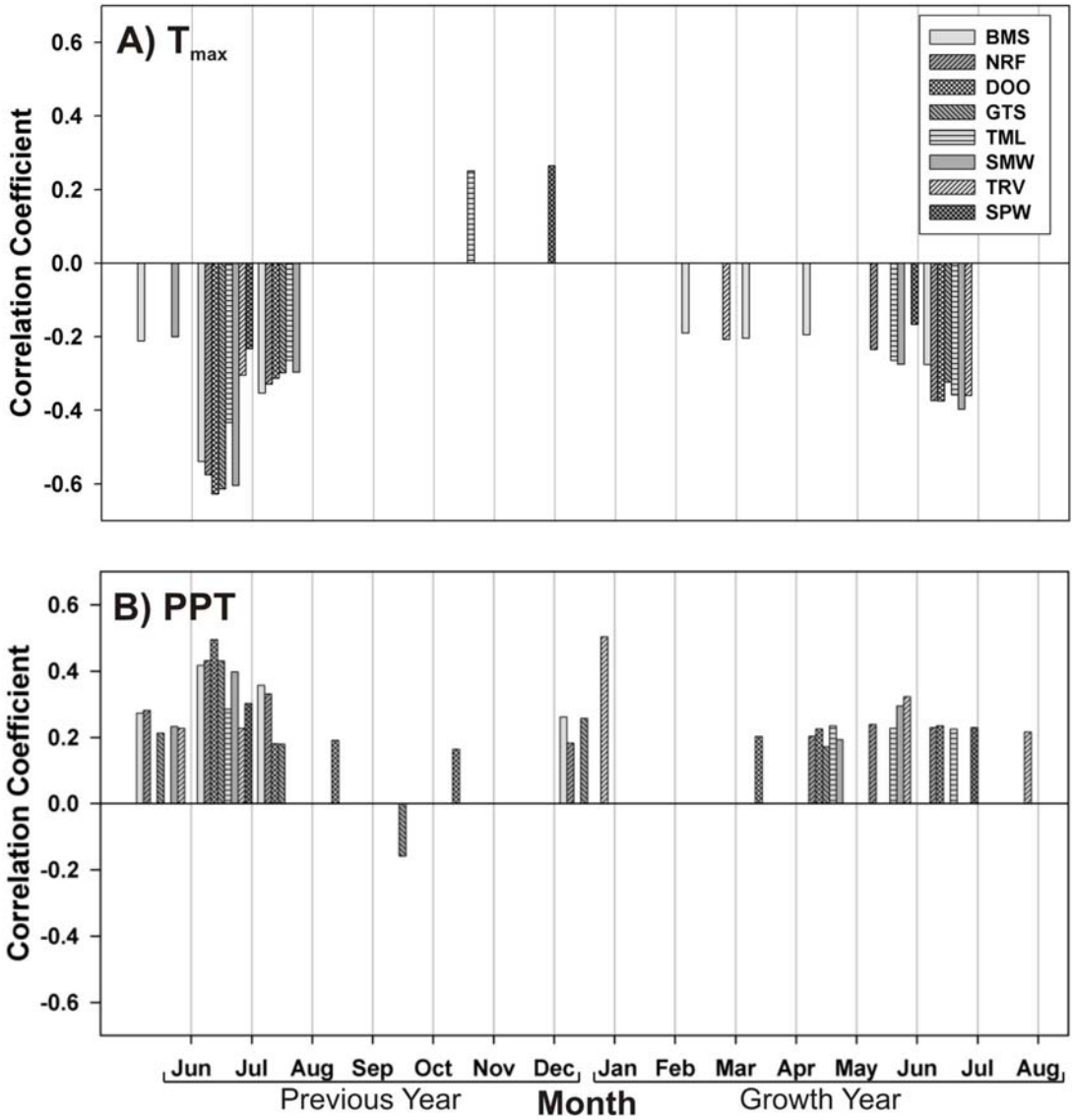

Figure 2.2. Correlations between all eight standardized ring-width chronologies and monthly temperature and precipitation over the 1900-2001 period. Analysis was carried out for: A) monthly mean maximum temperatures, and B) total monthly precipitation. Only correlations exceeding the 95% confidence limit when bootstrapped 1000 times are displayed.

PPT, with TRV, the chronology furthest east of the CD, displaying the strongest positive correlation (r = 0.50). Also, the pattern of monthly relationships (Figure 2.2*a*,*b*), and the observed 35 yr MCC's indicating temporal instability of individual months (*see* Appendix D), suggests the trees are most likely moisture sensitive over the summer season (June-August). Thus, a seasonal or annual combination of a climate index that integrates both temperature and precipitation (e.g. PDSI, MSD) may produce a stronger and temporally stable relationship.

Annualized climatic data and drought indices for 13 different 12-month periods resulted in lower overall correlations and decreased temporal stability of the climate/ring-width signal as indicated by the 35 yr MCC's displaying temporal gaps of non-significant correlation. These gaps of significant correlation consequently indicate a violation of the temporal stability assumption implicit to linear regression. Alternatively, all sites display stronger overall correlations with improved temporal stability to summer season T_{max} and PPT (Table 2.2; Appendix D). Table 2.2 highlights the moderate to strong correlations between each chronology and Kalispell MSD (r = 0.33-0.64) and summer PDSI (r = 0.25-0.62), thus supporting the notion that the chronologies are moisture sensitive during the growing season. Both MSD and PDSI exhibit the strongest relationship to chronologies located west of the CD, perhaps indicating that Kalispell precipitation records better represent this region. Summer PDSI calculated for Montana climate division data fails to improve the relationship with all chronologies, especially those east of the CD, and use of individual eastern climate records (Babb and Browning) for

calibration with eastern chronologies indicates the stations are largely unrepresentative of the eastern half of GNP.

Results from correlation analysis led me to initially select Kalispell MSD and summer PDSI for reconstruction. For the purpose of variable reduction, and investigation of inter-site variability, factor analysis was carried out on the standardized correlation matrix of all eight chronologies with *m* – the number of common factors the set of chronologies will be reduced to – set to four. Factor analysis indicates similarity between

Table 2.2. Seasonal correlations between all chronologies and summer Tmax, summer PPT, MSD, and summer PDSI for Montana climate division 1(MTdiv1) and Kalispell (Kal.). Correlation coefficients shown are the maximum values obtained from a lag 1 year relationship and are significant at the $p < 0.05$ level. Light (dark) gray shading indicates chronologies west (east) of the CD.

Site Code	Kal. Summer Tmax	Kal. Summer PPT	Kal. MSD	Kal. Summer PDSI	MTdiv1 Summer PDSI
BMS	-0.590	0.559	0.640	0.591	0.509
NRF	-0.589	0.569	0.631	0.622	0.491
DOO	-0.531	0.466	0.498	0.512	0.446
GTS	-0.538	0.451	0.502	0.493	0.407
TML	-0.455	0.320	0.368	0.361	0.318
SMW	-0.585	0.390	0.462	0.451	0.378
*TRV	-0.366	0.394	0.400	0.504	0.422
SPW	-0.302	0.306	0.327	0.250	0.199
Mean	-0.495	0.432	0.479	0.473	0.396

[a] Correlation coefficient not significant at ($p \leq 0.05$)

*TRV Correlation coefficient for growth year (current year)

chronologies by clustering factor loadings for western (BMS, NRF, DOO) and eastern (GTS, SMW, TML) chronologies on factors one and two respectively. TRV and SPW were found to be the sole significant loading on factors three and four representing their uniqueness from the GNP Douglas-fir chronologies and indicating their likelihood of

containing different climatic information (*see* Appendix A). Thus, TRV may represent a chronology located in a region climatically different from GNP with SPW indicating a potentially different response to climate over the growing season. Potential predictor chronologies (and factor scores) for use in MSD reconstructions, along with the appropriate lags (+/-2 yr), were selected using a "best subsets" procedure and added variable plots for entry into separate least squares regression models. The most parsimonious models were then chosen based upon the adjusted r^2 value, Mallow's C-P and S (root of mean squared error). Reconstructions using factor scores did not substantially improve the model (adjusted r^2 = 0.447, C-P = 5.8) and due to truncation at A.D. 1710 based on the shortest chronology (Table 2.1; SSS cutoff) I opted for the simpler multiple linear regression method using standardized chronologies as predictors.

Although both drought metrics are successfully reconstructed, summer PDSI was excluded from further analysis because of slightly reduced adjusted r^2 (PDSI = 0.395 vs. MSD = 0.443) and Mallow's C-P (PDSI = 5.0 vs. MSD = 4.3), indicating increased lack of fit in a 4-predictor model. Admittedly, reconstruction using either drought metric is justifiable and produces similar results, but the minor improvement in terms of variance explained and the simple computation and interpretation of MSD values resulted in selection of this moisture anomaly metric for reconstruction. The final two models were constructed using a combination of the BMS, SMW, TRV, and SPW chronologies as predictor variables:

$$MSD_1 = - 462 - 89.2\ (BMS)_t + 187\ (BMS)_{t-1} + 42.7\ (SMW)_t + 58.0\ (TRV)_t + 57.0\ (SPW)_t$$

$$MSD_2 = - 450 - 72.8\ (BMS)_t + 201\ (BMS)_{t-1} + 54.2\ (SMW)_t + 56.3\ (SPW)_t$$

Both of the reconstructions used the SSS value of 0.85 for the shortest chronology as the termination date for the early portion of the record. The chronologies and SSS termination dates for the longest reconstruction (MSD_2) are presented with sample depth through time in figure 2.3 (*a*,*b*,*c*). Consequently, the reconstructions span A.D. 1618-2000 and 1540-2000, and are based on 5 and 4 predictor variables respectively. In addition, the models based solely on the standardized chronologies produce almost identical reconstructions of moisture variability as those produced using factor analysis, thus confirming the robust nature of the reconstruction methods.

The stability of each MSD reconstruction was evaluated using standard parametric and nonparametric methods (*see* Fritts, 1976). Models were calibrated over the 1931-2000 interval to capture a portion of the severe 1917-1941 drought, thus avoiding extrapolation of values when verified over the 1900-1930 period. However, this method of data splitting provides a limited assessment of model stability due to drastic differences between the reconstructed and predicted portions. Hence, I circumvent such problems using a method - similar to the "leave-one-out" method (Gordon, 1982) - known as the predicted residual error sum of squares procedure (PRESS, [Draper and Smith, 1998]) for a stability assessment of the full model (1900-2000). Examination of the instrumental and predicted summer MSD indicates that the model successfully captures low-frequency variability and provides conservative estimates of interannual variability (Figure 2.4*a*). The reconstructions pass all model validation procedures obtaining significant ($p = 0.01$) results for the sign test and positive values for the reduction of error statistic (Table 2.3). Each reconstruction of MSD is highly correlated

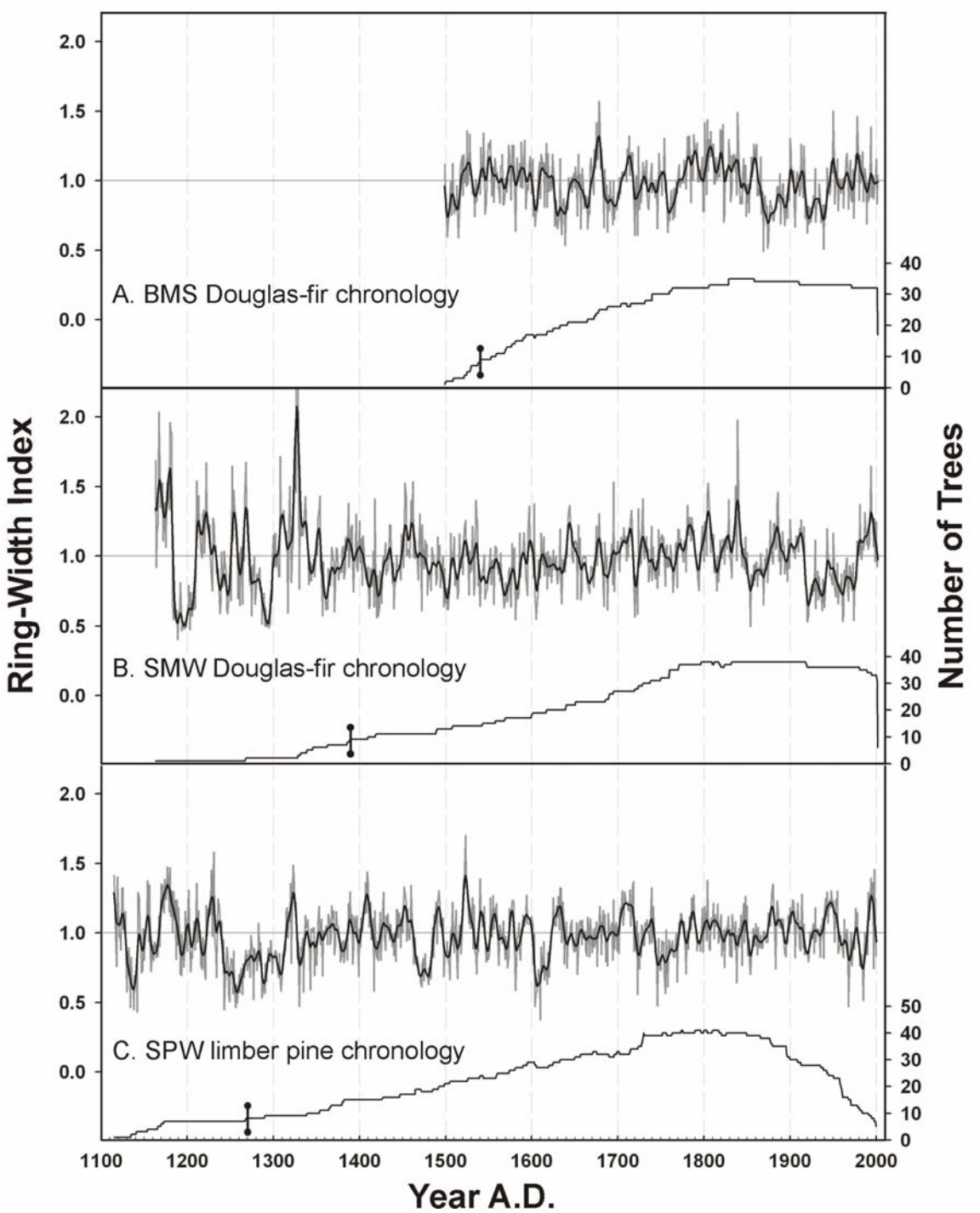

Figure 2.3. Standardized chronologies (gray line) smoothed with a 10 yr cubic spline (heavy black line) for (A) BMS, (B) SMW, and (C) SPW. Lower line indicates sample depth (number of trees) through time with subsample signal strength ≥ 0.85 indicated by a heavy, vertical black bar.

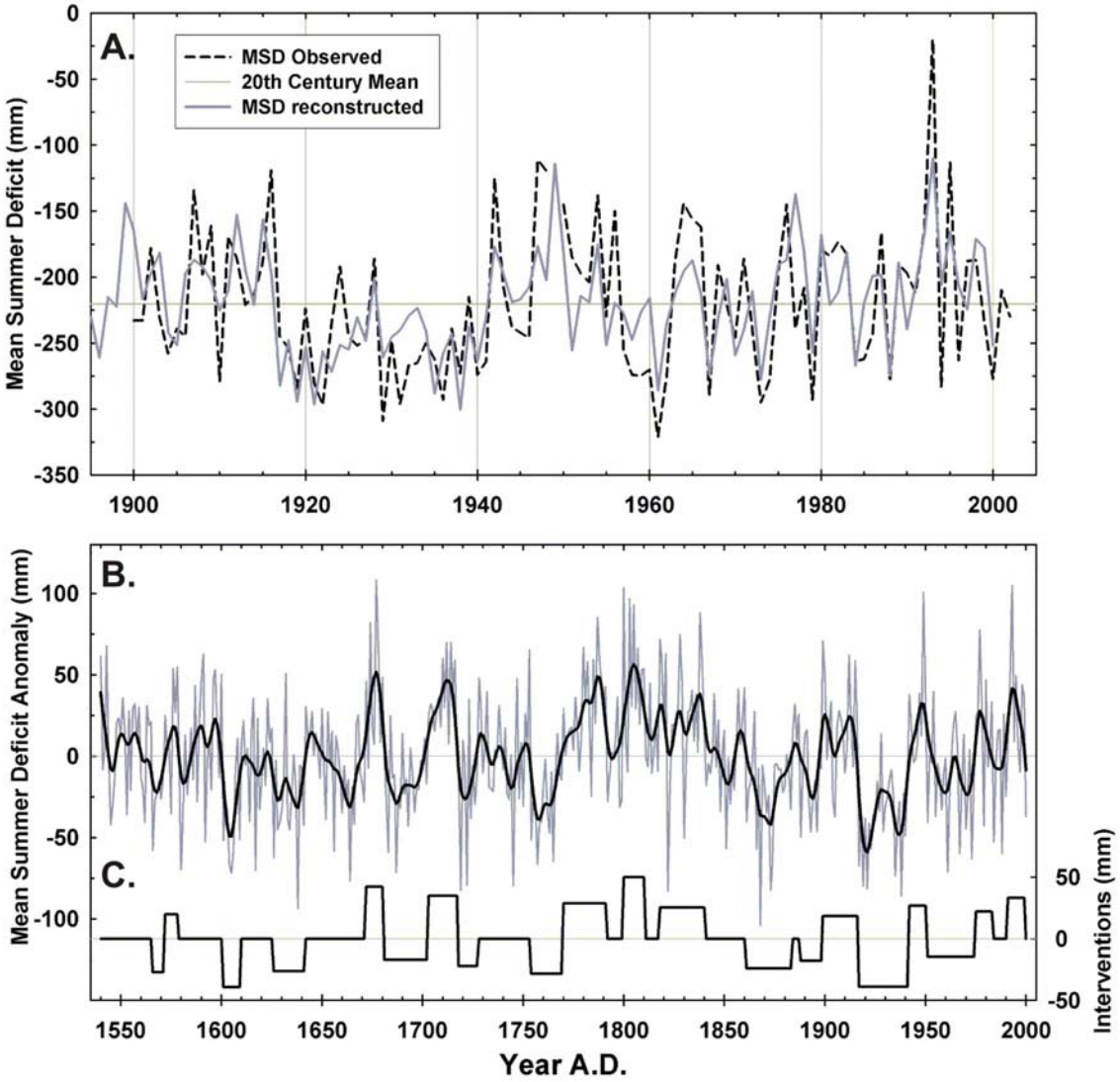

Figure 2.4. The summer drought reconstruction for Glacier National Park. (A) Comparison of the observed and reconstructed MSD records for the 1900-2000 calibration period. (B) Reconstructed MSD (dark gray line) smoothed with a 10 yr cubic spline (thick black line) spanning A.D. 1540-2000. (C) Decadal-scale drought regimes exhibiting the significant step-changes in the mean (event intensity) identified by the intervention model.

with the instrumental data, and the PRESS test indicates temporal stability of the drought/ring-width relationship. The Durban-Watson test detects no significant first-order autocorrelation, and examination of the normal quantile distribution and residual

plots shows all regression assumptions are met (Draper and Smith, 1998). Therefore, I hindcast MSD estimates back to A.D. 1540. Due to the similarity in reconstruction quality and validation statistics, further analysis and results will only be presented for the MSD_2 reconstruction.

Table 2.3. Regression model verification statistics for the full MSD_1 and MSD_2 reconstructions - including the calibration and verification periods.

Model	Period	n	r^2	r^2_{adj}	PRESS	r	RE[a]	Sign Test[b] (agree/dis.)	D-W[c]	S[d]
MSD_1	1900-2000	100	0.497*	0.470	PASS	0.71*	+0.50	75/25	1.93	39.6
Calibration	1931-2000	69	0.567*	0.533	PASS	0.75*	+0.43	51/18	1.95	39.6
Verification	1900-1930	31	0.384*			0.62*	+0.41	26/5		
MSD_2	1900-2000	100	0.466*	0.443	PASS	0.68*	+0.53	75/25	1.94	40.5
Calibration	1931-2000	69	0.504*	47.3	PASS	0.71*	+0.50	50/19	1.81	42.1
Verification	1900-1930	31	0.393*			0.63*	+0.60	24/7		

Verification tests were conducted by splitting the data into calibration and verification periods. To assess the stability of the of the model when calibrated over the full instrumental period the PRESS procedure (Draper and Smith, 1981) was used.

[a] RE is a highly sensitive measure of reconstruction reliability. Positive (negative) values of the statistic indicate successful (unsuccessful) reconstruction. (Fritts, 1976)

[b] Sign of departures for predicted and instrumental sample mean are significantly associated ($p < 0.01$)

[c] The Durban-Watson statistic indicates no significant serial correlation in the residuals ($p = 0.01$)

[d] The root mean squared estimate from the regression.

*Significant at $p = 0.01$ level.

Reconstructed Mean Summer Deficit, A.D. 1540 to 2000

The reconstruction of summer moisture variability since A.D. 1540 (Figure 2.4*b*) indicates the 20th century captures the full range of interannual variation with the exception of several severe single year droughts in the 19th and 17th centuries. The 20th century is equal to or greater than the previous four centuries for total number of single year severe (≤-1 standard deviation) and extreme (≤-2 standard deviation) droughts, though the 17th century is comparatively similar (Table 2.4). In contrast, the 18th and 19th

centuries appear to be dominated by many single year cool/wet events with 17 and 20 individual respective years greater than one standard deviation from the mean. The distribution of severe and extreme events in table 2.4 suggests that the 18th and 19th centuries were relatively wet when compared with the 17th and 20th centuries. Over the entire reconstruction, the clustering of extreme single year events alludes to the presence of a strong low-frequency persistence in the climate system.

Table 2.4. Number of extreme single year dry and wet events per century equal to or greater than +/- 1 and 2 standard deviations.

Century	Stdev +2	Stdev +1	Stdev -1	Stdev -2	Row Total
16th*	0	10	5	0	*
17th	2	4	19	2	27
18th	2	15	7	3	27
19th	4	16	8	3	31
20th	3	10	19	4	36
Total:	11	55	58	12	

*Record begins A.D. 1540

Analysis of decadal-scale deviations from the mean indicates long-duration regimes are common throughout the proxy summer moisture anomaly record (Figure 2.4*b*,*c*). Over the latter portion of the 20th century, intervention analysis detects 3 significant multi-year pluvial events - each lasting nine years with the 1991-1999 regime obtaining the greatest magnitude, and intensity (Table 2.5). However, comparison against previous decadal-scale wet events spanning A.D. 1540-1916 indicates these three regimes have been unremarkable in terms of duration, magnitude and intensity. In particular, the A.D. 1770-1791 and 1818-1840 regimes were most extraordinary in terms of duration and magnitude. Both regimes lasted more than 20 yrs, contain three single

Table 2.5. Decadal-scale dry (gray) and wet (white) regimes. Intervention analysis determined the significance of each regime (*p*-value), and duration describes the length of each regime (yrs). Magnitude identifies the severity of the mean departure for the entire duration, and intensity = magnitude/duration. The score of each event describes the overall strength of a moisture regime with higher values representing a stronger overall event.

Years	Condition	Intervention (*p* -value)	Duration	Magnitude	Intensity	Score
1566-1571	Dry	0.052*	6	-163.1	-27.2	15
1572-1578	Wet	0.055*	7	139.2	19.9	8
1601-1609	Dry	0.006	9	-354.5	-39.4	33
1626-1641	Dry	0.015	16	-420.4	-26.3	36
1672-1680	Wet	0.003	9	379.9	42.2	36
1681-1702	Dry	0.038	22	-377.8	-17.2	29
1703-1717	Wet	0.005	15	523.6	34.9	42
1718-1727	Dry	0.023	10	-222.1	-22.2	20
1754-1769	Dry	0.011	16	-453.9	-28.4	40
1770-1791	Wet	0.008	22	633.7	28.8	49
1800-1810	Wet	0.001	11	549.0	49.9	46
1818-1840	Wet	0.008	23	580.8	25.3	45
1861-1883	Dry	0.014	23	-556.9	-24.2	43
1888-1898	Dry	0.048	11	-197.6	-18.0	16
1899-1916	Wet	0.005	18	330.7	18.4	26
1917-1941	Dry	0.000	25	-978.7	-39.1	57
1942-1950	Wet	0.011	9	241.5	26.8	22
1951-1974	Dry	0.032	24	-352.5	-14.7	29
1975-1983	Wet	0.037	9	198.2	22.0	15
1991-1999	Wet	0.016	9	299.9	33.3	27

*Decreasing sample depth and borderline *p* -values suggests cautious interpretation.

year events greater than 2 standard deviations, and exhibit high magnitudes with moderately high intensities. Over the 20th century, the only substantially long pluvial event was the A.D. 1899-1916 regime spanning a total of 18 yrs. This regime corresponds to other decadal-scale wet regimes throughout the western U.S. and Canada (e.g. Fye et al., 2003; Watson and Luckman, 2004); however, in relation to other long-

duration (>10 yrs) pre-instrumental pluvial events, the A.D. 1899-1916 event had the lowest magnitude and intensity.

Prior to the 20th century, the single most intense decadal-scale wet regime spanned A.D. 1800-1810, with the 1672-1680 event obtaining a similar intensity with reduced duration and magnitude. Intensities for each pluvial regime are greater than one standard deviation from the reconstruction mean, with the 1800-1810 event obtaining an extraordinary 6 of 11 yrs above 1 standard deviation (3 of the 6 yrs surpassed 2 standard deviations). Overall, pluvial events of the 20th century have not been exceptional in the context of the past 461 yrs with figure 2.4 (*b*,*c*) indicating the A.D. 1550-1650 as the only period with fewer cool/wet decadal-scale events.

In contrast, decadal-scale droughts of the 20th century have been unprecedented when compared with long-duration dry events of the previous four centuries. In particular, the A.D. 1917-1941 drought obtains the overall greatest score of any single event within the reconstruction, thus signifying it is unequaled in terms of duration, magnitude, and intensity (Table 2.5). This single dry event encompasses over 25 yrs with 12 individual yrs less than -1 standard deviation from the mean, four of which reach extremely dry conditions for GNP surpassing -2 standard deviations. Only the three pluvial events that occurred over A.D. 1770-1840 obtain similar scores, thus placing the next greatest pre-instrumental drought (A.D. 1861-1883) in fifth position overall. The intensity of the 1917-1941 regime is -39.1, demonstrating the average for the 25 yr period exceeds one standard deviation from the reconstruction mean. Over the 461 yr period, only the drought of A.D. 1601-1609 was more intense. Although several droughts in the

instrumental and reconstructed record are similar in terms of duration, no single decadal-scale regime is comparable in magnitude.

Discussion

Summer Drought in Glacier National Park

The summer moisture anomaly reconstruction shows the prevalence of decadal-scale droughts and short-duration pluvial events after 1850. For instance, the 1917-1941 drought event was the most severe of the past 461 yrs, with the 1860-1883 drought being the second most severe. Contained within the aforementioned decadal-scale regime, however, lies the most extreme single-year drought in 1868. A succession of long-duration, high-intensity pluvial events, unsurpassed by any in the instrumental and reconstructed time series, occurs from 1770-1850. This succession of regimes coincides with the height of the Little Ice Age (LIA; ~14^{th}-19^{th} century A.D.) and glacial expansion within the park (Carrara and McGimsey, 1981). Prior to this time (1540-1770), summer conditions appear to fluctuate between drought and pluvial events with sustained periods of high-frequency variation around the long-term mean. Though the intervention detection algorithm requires additional data for detection, observation of instrumental records since 2000 indicate that summer drought in GNP has shifted to a severe warm/dry phase, which continued through the summer of 2003.

Proxy Reconstruction Comparison

Placing GNP within a larger spatial context, I investigate decadal-scale moisture variability and phasing along a north-south transect spanning the U.S. and Canadian

Rockies (Figure 2.5). Figure 2.5 identifies the reconstructions used in the comparison, along with the month, season, or annual period against which the records were calibrated. Dominant modes of variation in precipitation anomalies along the transect were established using the multi-taper method (MTM; Mann and Lees, 1996). Strong power in the frequency domain was tested against a red-noise background over a common interval (1540-termination of record), and only peaks exceeding the 95% confidence limit were considered significant. The series were then smoothed using a spline set to capture decadal modes of variation common to all reconstructions. Although differences in seasonality of each moisture proxy may seem to inhibit comparisons among the reconstructions, summer drought indices integrate precipitation over the winter and spring, and the majority of western chronologies retain some residual level of winter precipitation signal even though they are calibrated over the summer season (Stahle et al., 2000).

Each reconstruction was found to exhibit significant decadal and multidecadal variability in the 20-30 and >50 yr frequencies (see Appendix E). The consistency among the spectral characteristics in the decadal and multidecadal wavelengths suggests a common driver, or mechanism, forcing the regional or continental expression of drought/pluvial events. In addition, the many different species used in the hydroclimatic reconstructions implies that the low-frequency signals (inherent in western North American tree-ring based reconstructions of climate) do not extend from species-specific physiological traits. Instead, the observed modes of variation most likely extend from complex ocean-atmosphere teleconnections, such as the Pacific Decadal Oscillation

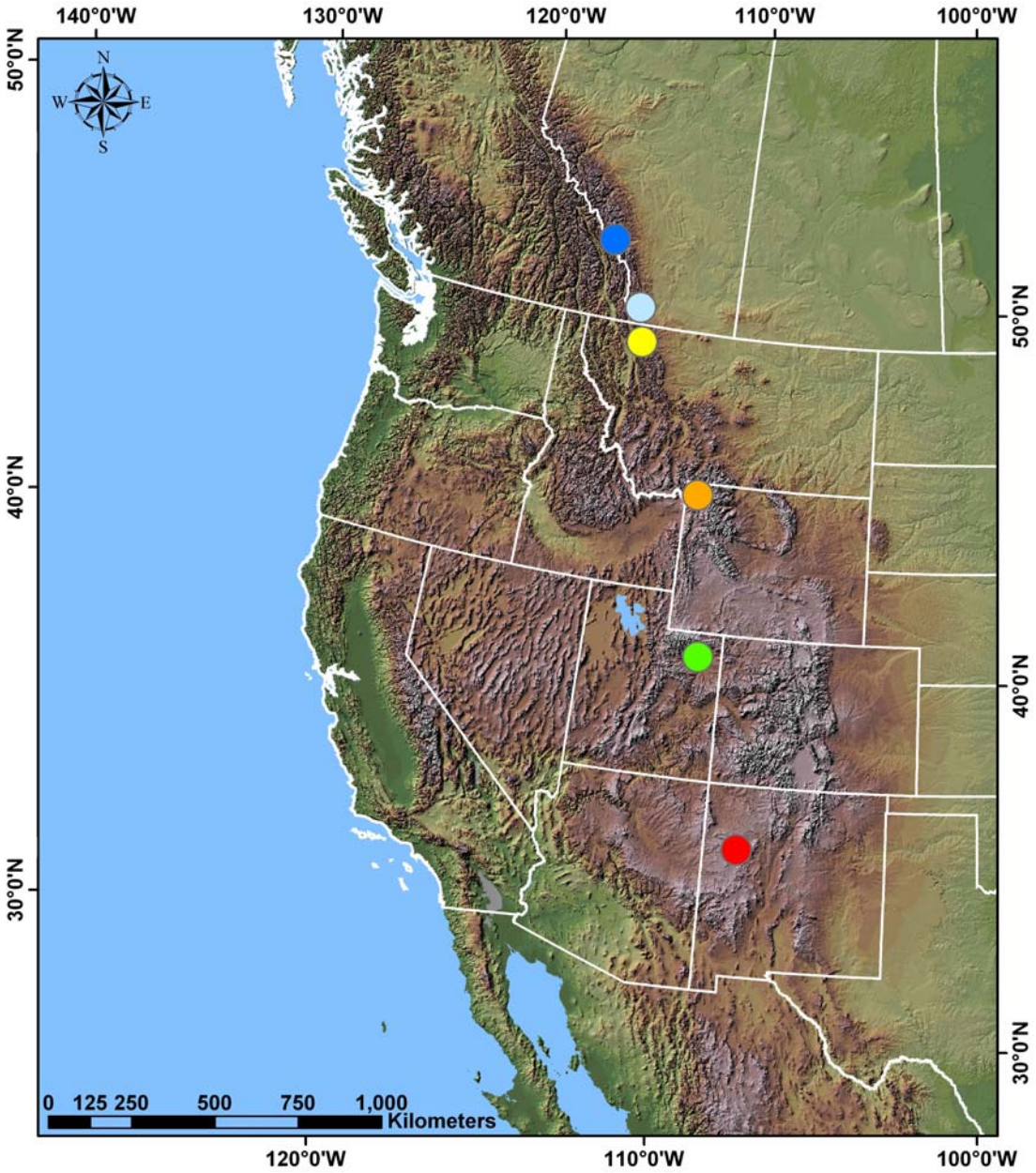

Figure 2.5. Location of tree-ring based precipitation and drought reconstructions used in comparison of moisture conditions along a north to south Rocky Mountain transect. Included reconstructions are: annual precipitation (pJuly-June) from Banff National Park (NP; dark blue circle) and Waterton NP (light blue circle), Alberta, Canada (Watson and Luckman, 2003); Glacier NP, Montana (this study) summer drought (yellow circle); annual (pJune-June) precipitation for northwestern Yellowstone NP, Wyoming (orange circle; Gray et al., 2003); Uinta Basin, Utah June PDSI (green circle; Gray et al. 2004); and annual precipitation (pJuly-July) for El Malpias National Monument (NM, red circle) in northwestern New Mexico (Grissino-Mayer, 1996).

(20-30 yr modes of variation; see Mantua and Hare, 2002) and Atlantic Multidecadal Oscillation (60-80 yr modes of variation; Enfield et al., 2001; Gray et al., 2003). Such ocean-atmosphere linkages provide a potential mechanism for understanding regional entrainment of drought events, and may also lead to the temporal and spatial migration of these moisture anomalies (Stahle et al., 2000; Gray et al., 2003).

Along the north to south Rocky Mountain transect, regional patterns of decadal-scale moisture variation emerge. Most striking is the 1550's to 1600's southwestern U.S. megadrought (Figure 2.6), which began during the 1540's in northwestern Mexico (Stahle et al., 2000). As first noted by Stahle et al. (2000), the drought is strongly expressed in the El Malpais precipitation reconstruction (Grissino-Mayer, 1996) with a gradual shift through time as the drought expanded northward. The onset of drought begins in the mid-1560's in the Uinta Basin, Utah (Gray et al., 2004), with a substantial delay before reaching Yellowstone NP, Wyoming (onset in the mid-1570's). In the northern Rocky Mountains, four possible 16th-century megadrought scenarios exist: 1) the drought is apparent in GNP as the weak 1566-1571 dry interval (Table 2.5) and in Banff National Park as the dry period spanning 1555-1585; 2) the megadrought did not begin in GNP until the intense 1601-1609 dry event while Banff remained in phase with the southwest; 3) the southwestern and northwestern regions of the U.S. are out of phase; or 4) the patterns are random. As described by Watson and Luckman (2004), a potential forcing mechanism that could explain the pattern described in scenario two may extend from zonal flows off the north Pacific. Such flows can result from prolonged, cool La

Niña-like conditions in the equatorial Pacific, and Stahle et al. (2000) suggest that these conditions likely occurred during the 16th-century megadrought.

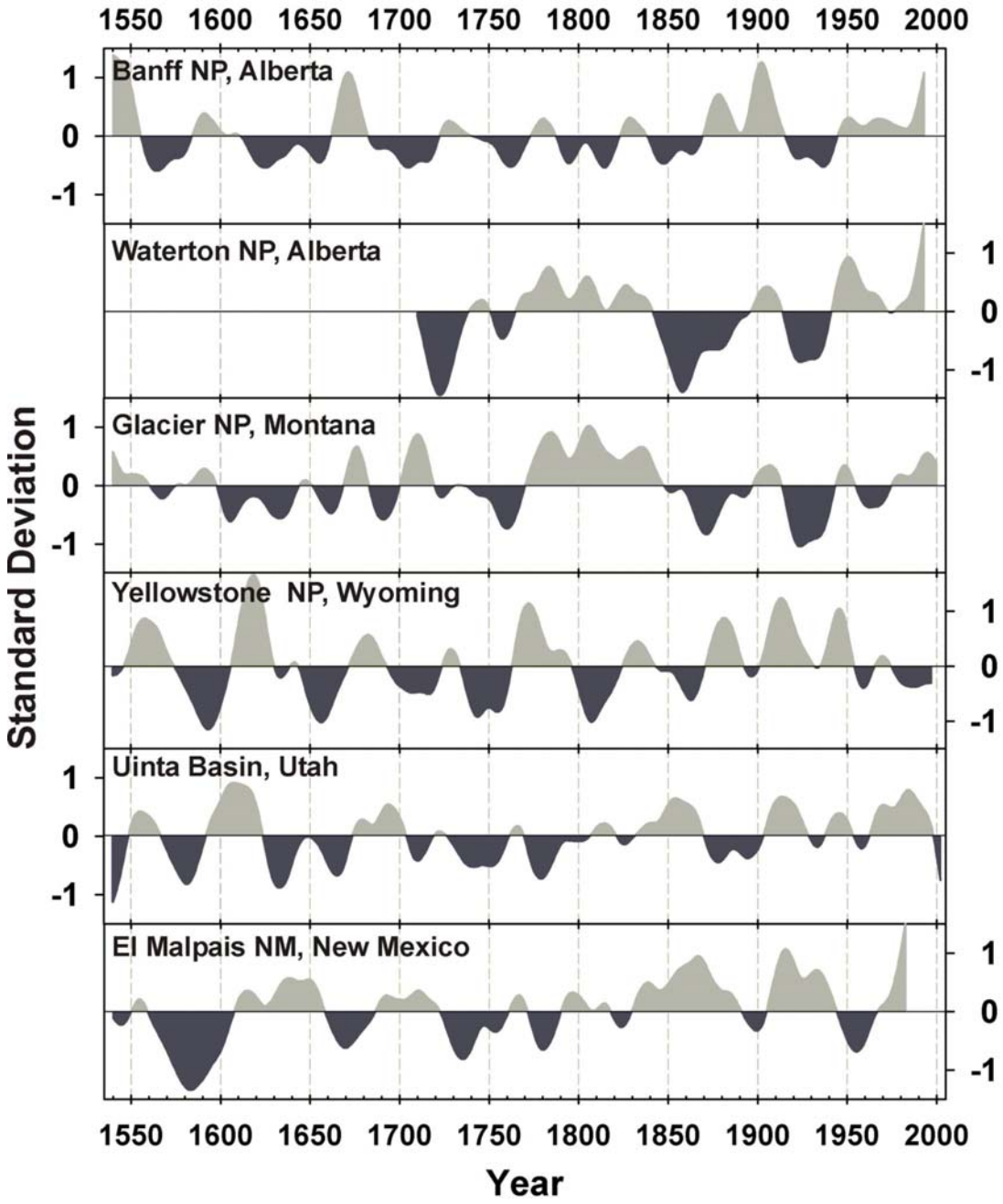

Figure 2.6. Tree-ring based reconstructions of moisture conditions along a north to south Rocky Mountain transect. Each series has been normalized and smoothed using a 25 yr cubic spline to highlight the prominent 20 to 30 yr frequencies identified by MTM spectral analysis (Mann and Lees, 1996).

Temporal and spatial shifting of other decadal-scale moisture events is evident among these reconstructions. For instance, an extremely wet period in Yellowstone NP and the Uinta Basin in the early 17th century is expressed to a lesser degree in El Malpais, while average to dry events were present in Glacier NP and Banff NP. Furthermore, shifts in intensity and timing occur among the severe droughts of the 1620-1650 period in Banff NP, Glacier NP, Yellowstone NP, and the Uinta Basin. However, during the 1650's the drought becomes spatially extensive and temporally analogous, extending from El Malpais, NM to Banff NP. Beginning in the 1670's, a strong wet regime is evident in Banff NP; however, this regime is reduced in intensity as it moves south. In addition, a temporal shift in date of onset occurs as the regime moves south, as it appears in El Malpais, NM around 1790. A shift back to a severe multidecadal drought occurs about 1720 in the Southwest and extends north to Banff NP. This drought appears to be most intense in the Southwest, while losing intensity and becoming shorter in duration north of Yellowstone NP.

Beginning in the 1770's, smaller-scale, or sub-regional, moisture patterns emerge. For instance, the LIA cool wet period from 1770-1840 is clearly evident in Glacier and Waterton National Parks, while an intense wet anomaly of shorter duration extends from 1770 to the mid-1790's in Yellowstone NP. Meanwhile, drought conditions dominate this period in the Uinta Basin and El Malpais, NM (Figure 2.6). A shift to strong pluvial events in the southwest occurs throughout the 1850-1860 time period, while dry conditions extend from Yellowstone NP through Banff NP during this time, including the central U.S. (Woodhouse and Overpeck, 1998). In fact, the 1860's drought emerges as

the most intense decadal-scale drought for numerous sites throughout the Canadian Cordillera (Watson and Luckman, 2004). Large-scale correlations once again appear in the early 20th century during the pluvial event centered around 1900, although the intensity of the event varies, with the lowest intensity present in the Glacier-Waterton region. It is interesting to note, however, that during the 1920-1940 time period, the southwest once again shifts into opposing phase with the northern Rockies, emphasizing the smaller-scale moisture patterns prevalent throughout the 1770-1900 period.

The 'megadrought' of the Pacific Northwest and the northern Rockies occurred over the first half of the 20th century (A.D. 1917-1941) and spans a total of 25 yrs (Figure 2.6). I classify this drought as the northwestern 'megadrought' due to its long duration and considerable spatial extent throughout the northern Rockies and the Pacific Northwest. Along the north-south transect, the 1917-1941 extreme drought regime appears to have been most intense in Glacier NP, and shows marked reductions in overall magnitude of moisture anomaly relative to long-term variations present in the Waterton NP and Banff NP reconstructions (Figure 2.6). For the northwestern U.S., Watson and Luckman (2004) found the 20th-century megadrought to be the most intense event in the past 300 yrs for the gridded PDSI reconstructions in Washington, Idaho, and Montana (Cook et al., 1999). Conversely, the early 20th-century drought is least intense over the northwestern portion of the Canadian Cordillera, and within the drought reconstruction network only the Jasper, Oliver, and Lillooet precipitation reconstructions identify the drought as the most extreme event over the entire length of the proxy record (Watson and Luckman, 2004). Overall, the 1917-1941 drought is exceptional due to its expression

across the northwest as the most extensive drought regime and because it preceded and encompassed the Dust Bowl years expressed across the U.S. and Canadian prairies.

Of particular significance with respect to the moisture reconstruction for Glacier NP is the consistency between moisture patterns in Glacier and Waterton National Parks. For example, GNP displays strong consistency with annual reconstructions of precipitation (previous July- current June) for the Canadian Rockies (Watson and Luckman, 2004), specifically Waterton National Park, though the intensity and magnitude of the events differ. In both moisture records, the end of the LIA is expressed as a long-duration wet event beginning in the 1770's and extending to the 1840's. However, the overall strength of the LIA event in GNP is greater in magnitude and intensity than the LIA in Waterton NP. Both parks show the onset of severe drought in the 1850's, extending through the 1890's; however, this drought is most extreme in Waterton NP and less so in Glacier NP. The early 20th century pluvial event (1899-1916) is of equal magnitude in both records, yet the drought of 1917-1941 – which encompasses the 'Dust Bowl' years – is the most extreme in GNP. The similarity between moisture variability in Glacier and Waterton National Parks demonstrates the robust nature of the reconstructions on a regional scale, while also suggesting differences in spatial expression of moisture variability.

Conclusions

The results of my research indicate that within GNP the end of the LIA was marked by a series of three long-duration, high-magnitude pluvial events spanning

approximately 70 years. Post A.D. 1840 the climate shifted to severe decadal-scale droughts that extended up to a weak early 20th century pluvial event covering A.D. 1899-1916. The drought of A.D. 1917-1941 obtained the greatest overall magnitude and duration of any single decadal-scale event experienced over the 461 yr reconstruction. Furthermore, the 1917-1941 drought was primarily expressed throughout the northern Rockies and the Pacific Northwest, and encompasses the 1930's Dust Bowl event that had devastating effects on the U.S. and Canadian Prairies. Much like the 16th-century megadrought in the Southwest, the spatial consistency of the early 20th-century drought across northern regions is striking, even though it did not always exceed the magnitude of events experienced over previous centuries.

The expression of drought along a north to south Rocky Mountain transect suggests GNP is most similar climatically to the Canadian Rockies. Moisture-sensitive reconstructions extending from the U.S. southwest to the northern Canadian Rockies indicate a common climatic forcing due to similar dominant modes of variation in the 20-30 and >50 yr wavelengths. Thus, the common modes of low-frequency variation in drought coupled with their migration through space and time suggests complex ocean-atmosphere teleconnections as a potential mechanism. As a consequence, it seems likely the prevalent long-duration shifts in climate throughout the western U.S. and Canada have played a large role in driving physical and ecosystem processes. Thus, future studies should seek to address the impacts decadal-scale variations in climate may have on physical processes - such as glaciers - and ecosystems. As well, investigating the role of ocean-atmosphere teleconnections as a driver of spatial and temporal variations in

drought may provide insight into specific mechanisms resulting in low-frequency moisture anomalies, and eventually allow for the long-term prediction of such events.

REFERENCES CITED

Biondi, F., 1997. Evolutionary and moving response functions in dendroclimatology. *Dendrochronologia* 15, 139-150.

Biondi, F., Kozubowski, T.J., Panorska, A.K., 2002. Stochastic modeling of regime shifts. *Climate Research* 23, 23-30.

Box, G.E.P., Jenkins, G.M., 1970. *Time series analysis: Forecasting and control*. Holden-Day Publishers, New York.

Box, G.E.P., Tiao, G.C., 1975. Intervention analysis with applications to economic and environmental problems. *Journal of the American Statistical Association* 70, 70-79.

Briffa, K.R., Jones, P.D., 1990. Basic chronology statistics and assessment. In: Cook, E.R., and Kairiukstis, L.A. (Ed.), *Methods of Dendrochronology: Applications in the Environmental Sciences*. Kluwer, Dordrecht, pp. 137-152.

Case, R.A., MacDonald, G.M., 1995. A dendroclimatic reconstruction of annual precipitation on the western Canadian prairies, since A.D. 1505 from *Pinus flexilis* James. *Quaternary Research* 44, 267-275.

Carrara, P.E., McGimsey, R.G., 1981. The late-neoglacial histories of the Agassiz and Jackson Glaciers, Glacier National Park, Montana. *Arctic and Alpine Research* 13(2), 183-196.

Cayan D.R., Dettinger, M.D., Diaz, H.F., Gram, N.E., 1998. Decadal variability of precipitation over western North America. *Journal of Climate* 11, 3148-3166.

Cunningham, C., 1982. Montana weather. *Montana Magazine*. Helena, Montana.

Cook, E.R., 1985. A time series analysis approach to tree-ring standardization. *PhD thesis*. University of Arizona, Tucson.

Cook, E.R., Kairiukstis, L. (Eds.), 1990. *Methods of Dendrochronology: Applications in the Environmental Sciences*. Kluwer, Dordrecht.

Cook, E.R., Shiyatov, S., Mazepa, V., 1990. Estimation of the mean chronology. In: Cook, E.R., Kairiukstis, L.A. (Eds.), *Methods of Dendrochronology: Applications in the Environmental Sciences*. Kluwer, Dordrecht, pp. 123-132.

Cook, E.R., Briffa, E.R., Meko, K.R., Graybill, D.A., Funkhouser, G., 1995. The 'segment length curse' in long tree-ring chronology development for paleoclimatic studies. *The Holocene* 5, 229-237.

Cook, E.R., Meko, D.M., Stahle, D.W., Cleaveland, M.K., 1996. Tree-ring reconstructions of past drought across the coterminous United States: tests of regression method and calibration/verification results. In: Dean. J.S., Meko, D.M., Swetnam, T.W. (Eds.), *Tree rings, environment and humanity*. Radiocarbon, Department of Geosciences, The University of Arizona, Tucson, pp. 155-169.

Cook, E.R., Meko, D.M., Stahle, D.W., Cleaveland, M.K., 1999. Drought reconstructions for the continental United States. *Journal of Climate* 12, 1145-1162.

Downing, D.J., McLaughlin, S.B., 1990. Detecting shifts in radial growth by use of intervention detection. In: Cook, E.R., Kairiukstis, L.A. (Eds.), *Methods of Dendrochronology: Applications in the Environmental Sciences*. Kluwer, Dordrecht, pp. 258-270.

Draper, N.R., Smith, H., 1998. *Applied regression analysis* (third edition). Wiley, New York.

Easterling, D.R., Karl, T.R., Mason, E.H., Hughes, P.Y., Bowman, D.P., Daniels, R.C., Boden, T.A. (Eds.), 1996. *United States historical climatology network (U.S. HCN) monthly temperature and precipitation data*. Carbon Dioxide Information Analysis Center, Oak Ridge National Laboratory, Oak Ridge, Tennessee.

Enfield, D.B., Mestas-Nunez, A.M., Trimble, P.J., 2001. The Atlantic multidecadal oscillation and its relation to rainfall and river flows in the continental U.S. *Geophysical Research Letters* 28(10), 2077-2080.

Finklin, A.I., 1986. *A climatic handbook for Glacier National Park – with data for Waterton Lakes National Park*. USDA Forest Service, Intermountain Research Station General Technical Report INT-204.

Fritts, H.C., 1976. *Tree Rings and Climate*. Academic Press, London.

Fye, F.K., Stahle, D.W., Cook, E.R., 2003. Paleoclimatic analogs to twentieth-century moisture regimes across the United States. *Bulletin of the American Meteorological Society* 84, 901-909.

Garfin, G.M., Hughes, M.K., 1996. *Eastern Oregon divisional precipitation and Palmer Drought Severity Index from tree-rings*. Report to the U.S. Forest Service Intermountain Research Station.

Gordon, G.A., 1982. Verification of dendroclimatic reconstructions. In: Hughes, M.K., Kelly, P.M. Pilcher, J.R., LaMarche, V.C. JR (Eds.), *Climate from tree rings*. Cambridge University Press, Cambridge, pp. 58-61.

Gedalof, Z., Smith, D.J., 2001. Interdecadal climate variability and regime-scale shifts in Pacific North America. *Geophysical Research Letters* 28, 1515-1518.

Gray, S.T., Betancourt, J.L., Fastie, C.L., Jackson, S.T., 2003. Patterns and sources of multidecadal oscillations in drought-sensitive tree-ring records from the central and southern Rocky Mountains. *Geophysical Research Letters* 30(6), doi:10.1029/2002GL016154.

Gray, S.T., Jackson, S.T., Betancourt, J.L., 2004. Tree-ring based reconstructions of interannual to decadal precipitation variability for northeastern Utah. *Journal of American Water Resources*, in press.

Graumlich, L.J., Brubaker, L.B., 1986. Reconstruction of annual temperature (1590-1979) for Longmire, Washington, derived from tree rings. *Quaternary Research* 25, 223-234.

Grissino-Mayer, H.D., 1996. A 2129 year annual reconstruction of precipitation for northwestern New Mexico, USA. In: Dean, J.S., Meko, D.M., Swetnam, T.W. (Eds.), *Tree Rings, Environment, and Humanity*. Radiocarbon, Department of Geosciences, The University of Arizona, Tucson, 191-204.

Grissino-Mayer, H.D., R.L., Holmes, Fritts, H.C., 1997. *The International Tree-Ring Data Bank Program Library, version2.1, users manual*. Tucson, Arizona.

Hare, S.R., Francis, R.C., 1994. Climate change and salmon production in the northeast Pacific Ocean. In: Beamish, R.J. (Ed.), *Climate Change and Northern Fish Populations. Canadian Special Publication of Fisheries and Aquatic Sciences*. National Academy Press, Washingtion D.C., pp.121.

Luckman, B.H., Briffa, K.R., Jones, P.D., Schweingruber, F.H., 1997. Summer temperatures at the Columbia Icefield, Alberta, Canada, 1073-1987. *The Holocene* 7, 375-389.

Mann, M.E., Lees, J.M., 1996. Robust estimation of background noise and signal detection in climatic time series. Climatic Change 33, 409-445.

Mantua, N.J., Hare, S.R., 2002. The Pacific Decadal Oscillation. *Journal of Oceanography* 58, 35-44.

McCabe, G.J., Dettinger, M.D., 2002. Primary modes and predictability of year-to-year snowpack variations in the western United States from teleconnections with Pacific Ocean climate. *Journal of Hydrometeorology* 3, 13-25.

Newhall, F., Berdanier, C.R., 1996. Calculation of soil moisture regimes from the climatic record. *Soil Survey Investigations Report 46,* USDA Natural Resources Conservation Service, Washington, D.C.

Palmer, W.C., 1965. Meteorological drought. *Weather Bureau Research Paper 45*, U.S. Department of Commerce, Washington, D.C.

Sauchyn, D.J., Beaudoin, A.B., 1998. Recent environmental change in the southwestern Canadian Plains. *The Canadian Geographer* 42, 337-353.

Selkowitz, D.J., Fagre, D.B., Reardon, B.A., 2002. Interannual variations in snowpack in the crown of the continent ecosystem. *Hydrological Processes* 16, 3651-3665.

Stahle, D.W., Cook, E.R., Cleaveland, M.K., Therrell, M.D., Meko, D.M., Grissino-Mayer, H.D., Watson, E., Luckman, B.H., 2000. Epic 16th century drought over North America. *EOS, Transactions, American Geophysical Union* 81, 121-125.

St. George, S., Luckman, B.H., 2001. Extracting a paleotemperature record from *Pica englmanii* treeline sites in the central Canadian Rockies. *Canadian Journal of Forest Research* 31, 457-470.

Stokes, M.A., Smiley, T.L., 1968. *An introduction to tree-ring dating*. University of Chicago Press, Chicago.

Thornthwaite, C.W., 1948. An approach towards a rational classification of climate. *Geographical Review* 38, 55-102.

Watson, E., Luckman, B.H., 2001. Dendroclimatic reconstruction of precipitation for sites in the southern Canadian Rockies. *The Holocene* 11, 203-213.

Watson, E. Luckman, B.H., 2003. Tree-ring based reconstructions of precipitation for the southern Canadian Cordillera. *Climatic Change,* (In press).

Wigley, T.M.L., Briffa, K.R., Jones, P.D., 1984. On the average of correlated time series, with applications in dendroclimatology and hydrometeorology. *Journal of Climate and Applied Meteorology* 23, 201-213.

Wilson, R.J.S., Luckman, B.H., 2003. Dendroclimatic reconstruction of maximum summer temperatures from upper treeline sites in Interior British Columbia, Canada. *The Holocene* 13(6), 851-861.

Woodhouse, C.A., Overpeck, J.T., 1998. 2000 years of drought variability in the central United States. *Bulletin of the American Meteorological Society* 79, 2693-714.

CHAPTER 3

DECADAL-SCALE CLIMATE DRIVERS FOR GLACIAL MASS BALANCE IN GLACIER NATIONAL PARK, MONTANA, USA

Introduction

As in the majority of the world's temperate, continental regions, alpine glaciers throughout the Rocky Mountains of the northern United States and southern Canada are currently experiencing a substantial decrease in number and extent (Luckman, 2000; Hall and Fagre, 2003). Glacier National Park (GNP), Montana (Figure 3.1) offers numerous examples of this pattern, including over 110 recently absent glaciers, with the remaining 40 glaciers disappearing rapidly (Carrara and McGimsey, 1981). Evidence from dated moraines and forest trimlines also shows that this retreat follows a significant Little Ice Age (LIA) advance that was otherwise unprecedented in the late Holocene (Carrara, 1989).

Though much is known about the mid- to late-20th century dynamics of glaciers in the Northern Rockies, there has been little exploration of the regional climatic conditions that drove their LIA advance or the late-19th and early-20th century transition to ablation-dominated modes. Here I compare documented advances and retreats for the extensively studied Jackson and Agassiz glaciers in GNP (Figure 3.1) with tree-ring based reconstructions of climate indices related to summer ablation potential (Chapter 2). Fluctuations in snowpack for the U.S. Northern Rockies, the primary driver of glacial accumulation rates, are strongly linked to the Pacific Decadal Oscillation (PDO; see

Mantua and Hare [2002]), with negative modes correlating with increased snow depth and snow water equivalent (SWE) (McCabe and Dettinger, 2002). Therefore, I link regional drivers of summer ablation with proxies for Pacific basin forcings of winter accumulation (PDO reconstruction; see D'Arrigo et al., [2001]) to produce a comprehensive picture of long-term glacial mass balance. Furthermore, I utilize the long-duration of these accumulation and ablation proxies to explore how decadal-scale variability in regional and Pacific basin climate influences glacial dynamics in GNP.

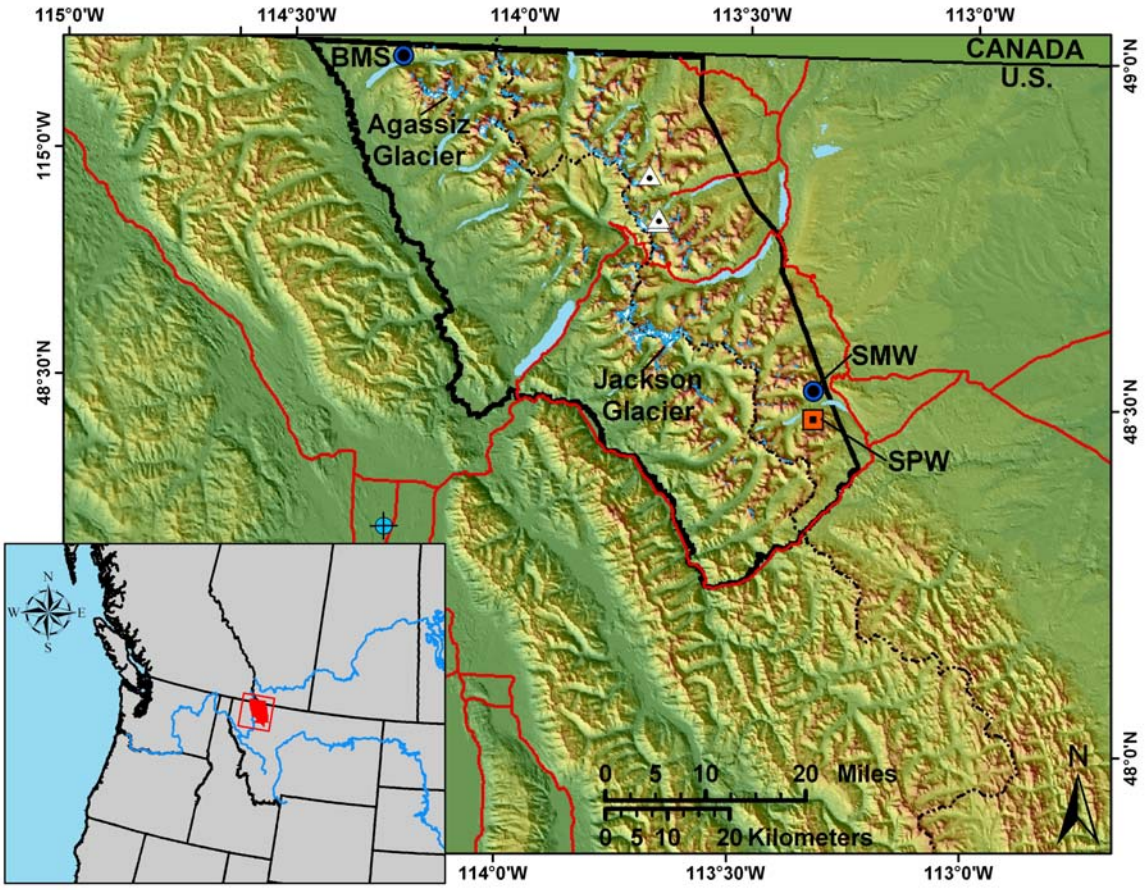

Figure 3.1. Location of glaciers, tree-ring chronologies (Douglas-fir [blue dotted circle], limber pine [orange dotted square]), snow courses (white dotted triangles) and the Kalispell meteorological station (blue circle w/crosshairs).

Data and Study Area

Here I utilize the terminus position chronologies of Carrara and McGimsey (1981) to represent post-Little Ice Age and 20th century dynamics for the Jackson and Agassiz glaciers (Figure 3.1). These chronologies were developed from tree-ring dating (n = 116) of multiple terminus positions (n = 21) for these glaciers during their retreat from LIA forest trimlines. National Park Service observations and repeat photography were also used in the development of the chronologies. These records provide us with a general representation of extent and retreat rates through time, unfortunately actual mass balance measurements are not available.

In a related study (Chapter 2), I used tree-ring data to reconstruct Mean Summer Deficit (MSD; [Newhall and Berdanier, 1996]) based on Kalispell, Montana meteorological records (Figure 3.1). The MSD reconstruction is used here as a proxy for summer (JJA) ablation extending back to A.D. 1540. MSD was chosen to represent summer ablation because this index, calculated as precipitation minus potential evapotranspiration, incorporates both temperature and moisture variability into a single metric. Moreover, for the GNP study area, MSD is strongly governed by mean summer maximum temperatures (r = -0.827), and summer temperatures alone have been shown to drive a large proportion of the variation in mass balance (Brathwaite and Olesen, 1989). The reconstruction was based upon a subset of the longest Douglas-fir (*Pseudotsuga menziesii* [Mirb.] Franco) and limber pine (*Pinus flexilis* James) tree-ring chronologies available for the area (Figure 3.1). The most parsimonious MSD reconstruction was

produced using a transfer function model designed to preserve low- and high-frequency variation (Cook et al., 1990). See chapter 2 for additional details.

Initial investigation of winter snowpack (accumulation) involved establishing the spatial relationships between North Pacific variability and winter precipitation by correlating October-March U.S. climate division data with the PDO index (http:/www.cdc.noaa.gov/USclimate/). Relationships between standardized SWE and PDO were then assessed using GNP snow course data (Figure 3.1) over the 1922-2000 common period (methods adapted from Selkowitz et al., [2002]). For a pre-instrumental perspective of variations in the PDO I chose the D'Arrigo et al. (2001) A.D. 1700-1979 reconstruction over other available reconstructions (e.g. Biondi et al., 2001) because it utilized the largest spatial network of chronologies, included proxies that integrated temperature and precipitation signals, and produced stronger calibration and verification statistics than previous reconstructions.

Multidecadal Variations in Summer Drought

Previous studies using instrumental records have suggested that summer drought in the western U.S. contains significant decadal and longer scale behavior (e.g. Cayan et al., 1998) that may have profound impacts on the long-term forcing of glacial dynamics. Here, the 461 yr reconstruction of MSD (Figure 3.2*a*) was analyzed using wavelet analysis to explore the low-frequency characteristics of drought for the study region in both the instrumental and pre-instrumental periods. Wavelet analysis employed the Morlet wavelet and zero padding, allowing for investigation of localized changes in

decadal modes of variability within the time series (Torrence and Compo, 1998). The MSD reconstruction exhibits significant multidecadal periodicities in the 16-32 yr and >64 yr domain (Figure 3.2*b*). Figure 3.2 shows that the A.D. 1630-1750 interval has the strongest significant power in the 16-32 yr wavelengths due to rapid shifts from strong summer pluvial (cool/wet) events to sustained droughts. As the end of the LIA

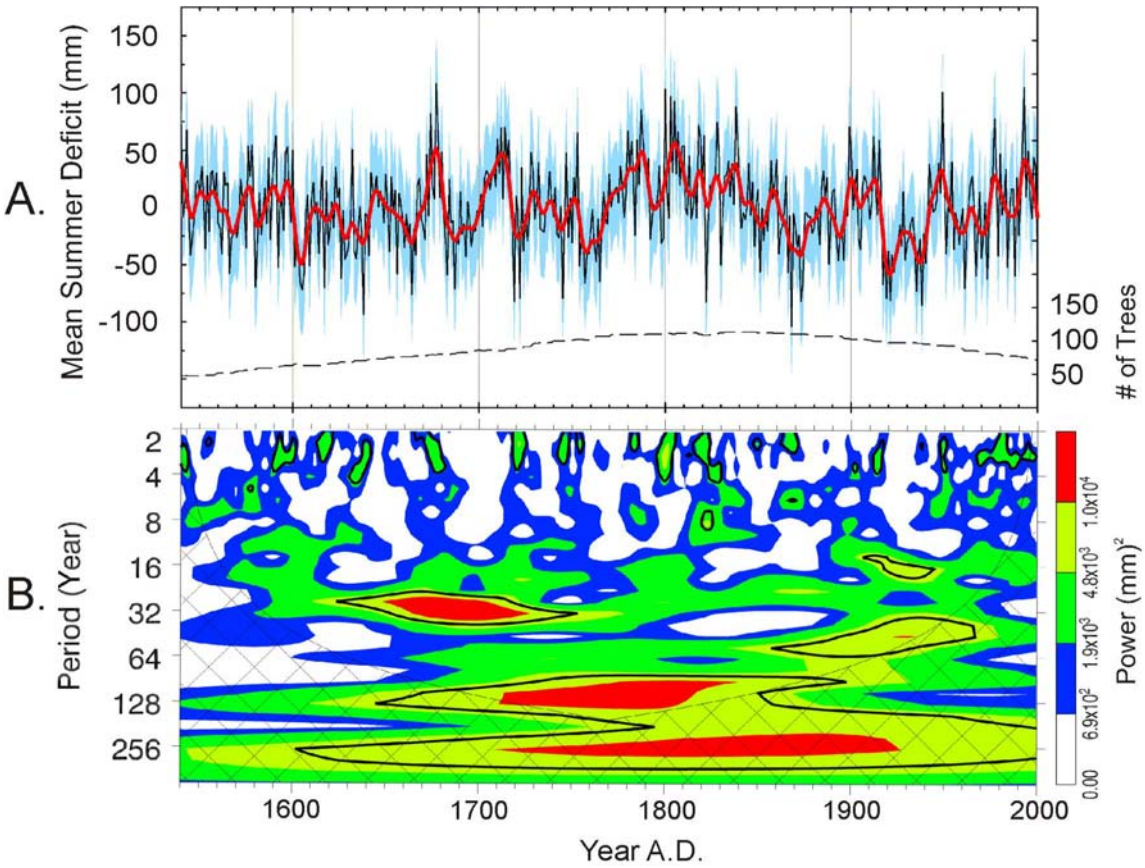

Figure 3.2. Summer drought reconstruction (Mean Summer Deficit) for GNP. (A) Summer drought reconstruction (black line) overlain with a 10 yr cubic spline (thick red line), confidence bands representing root mean squared error estimates (light blue), and sample depth (below). (B) The wavelet power spectrum for the summer drought reconstruction. Colored intervals represent 75, 50, 25, and 5% of the wavelet power, respectively. The black contour represents the 95% confidence level (compared to red-noise), and the crosshatched region indicates areas where zero padding has reduced the variance. Software provided by C. Torrence and G. Compo (available at; http:/paos.colorado.edu/research/wavelets/).

approached (~A.D. 1750-1850), power in wavelengths >64 yrs increased, coinciding with a series of long duration pluvial events spanning A.D. 1770-1840. From A.D. 1850 forward the climate shifts to higher intensity droughts of greater length than any experienced in the preceding 310 yrs, which corresponds with a shift to 32-64 yr frequencies. The observed multidecadal shifts in MSD coincide with known shifts in glacial margins (Figure 3.3*a*,*b*). However, accounting for ablation alone when inferring shifts in positive and negative mass balance may bias results if winter precipitation cannot be assumed constant.

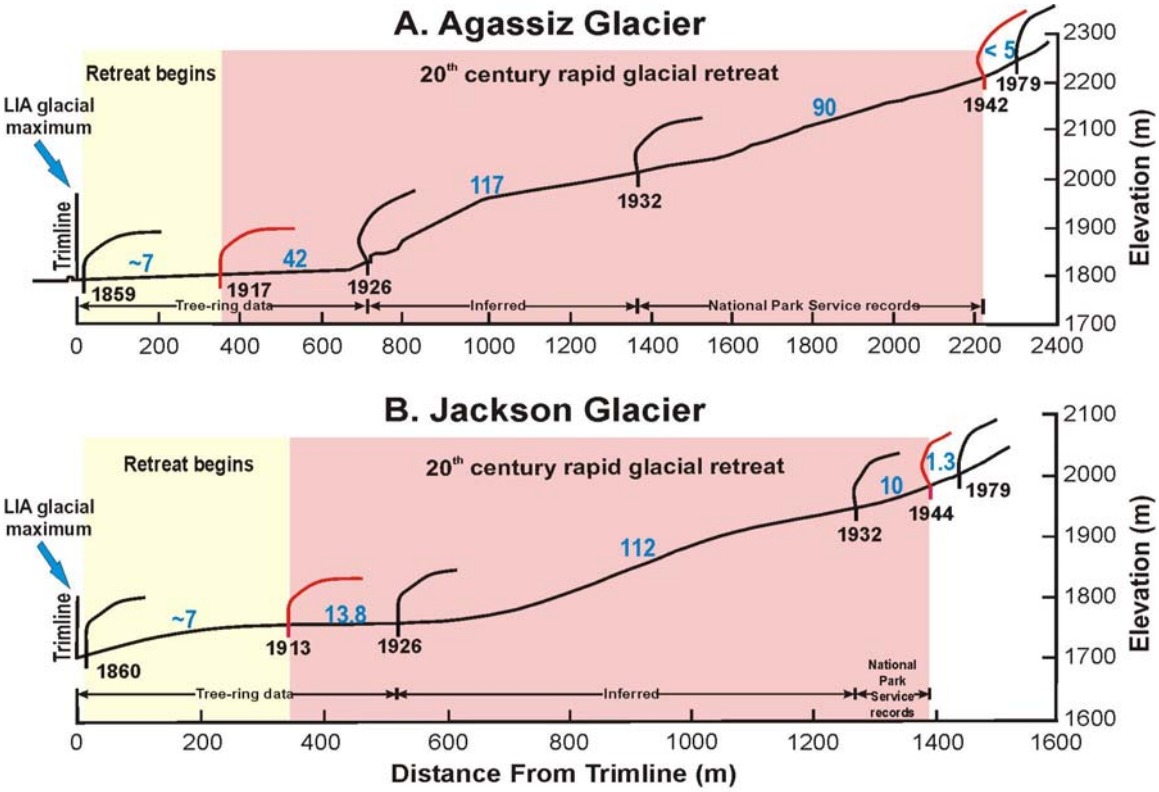

Figure 3.3. Profiles of the Agassiz (A) and Jackson Glaciers (B) showing the elevation of their terminus positions through time (modified from Carrara and McGimsey [1981]). Black lines represent key observations of glacial margins, and red lines highlight changes in glacial position between the onset and termination of the severe 1917-1941 drought. Blue font indicates estimated retreat rates (m/yr).

Linking Summer Drought and North Pacific Basin Variability to Glacial Dynamics

Significant changes in winter mass balance of glaciers in Washington, Alaska, Western Canada, and the Southern Cascades have been connected to low-frequency synoptic patterns linked to the Pacific basin (e.g. McCabe and Fountain, 1995; Hodge et al., 1998; and Bitz and Bittaisti, 1999). Within GNP, April 1st and May 1st snowpack fluctuations exhibit such low-frequency shifts in accumulation connected specifically to the PDO (Selkowitz et al., 2002); thus, winter snowpack serves as an exaggerating or moderating variable in annual glacial mass balance dynamics. The relationship between the PDO and precipitation in western Montana is greatest during the winter months (October-March), and is exhibited by the strong negative correlations for the region (*see* inset, Figure 4). A comparison between the smoothed annual PDO index and local May 1st SWE measurements from GNP (Figure 3.4*a*) indicate a strong inverse relationship (r = -0.764, r^2_{adj} = 57.9). Assuming this connection has remained stationary prior to instrumental records allows us to make inferences about low-frequency variations in snowpack using the normalized PDO reconstruction from D'Arrigo et al. (2001) as a proxy.

Comparing both the PDO and MSD reconstructions for GNP indicates that the maximum glacial advance near the end of the LIA coincides with an extended period where conditions in the North Pacific likely contributed to high winter snowpack coupled with little potential for significant summertime ablation (e.g. A.D. 1770-1790 and 1800-1830; Figure 3.4*b*,*c*). After A.D. 1850 long periods (1860-1890) of poor winter accumulation (warm North Pacific) and high summer ablation overlap, producing

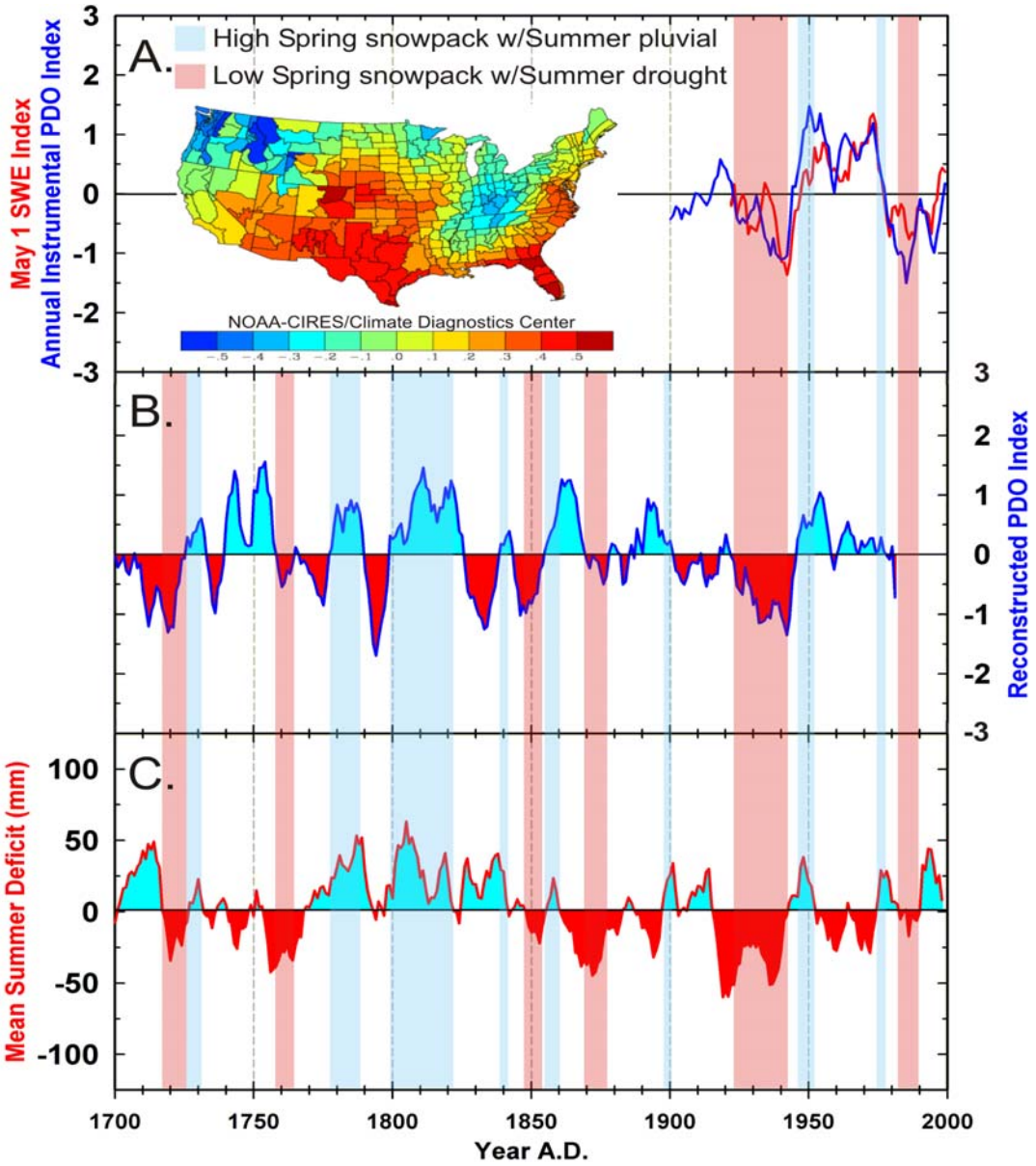

Figure 3.4. Comparison of GNP summer drought, winter snowpack and the Pacific Decadal Oscillation. The inverse of the instrumental and reconstructed PDO index is presented here for ease of comparison, and all time series have been smoothed using a 5 yr moving average. (A) Relationship between the average annual PDO index (blue line) (Mantua and Hare, 2002) and May 1st SWE index (red line) for GNP. (Inset) Seasonal correlations between winter (October-March) precipitation and the PDO index for all U.S. climate division data spanning 1949-2003. (B) Annual PDO reconstruction (D'Arrigo et al., 2001) used to infer positive and negative snowpack anomalies to A.D. 1700. The PDO reconstruction exhibits a strong relationship with the May 1st SWE index (r = -0.688, r^2_{adj} = 46.5) for the common period of overlap. (C) Summer drought reconstruction for GNP.

conditions favorable for negative annual mass balance and the start of glacial retreat. The glaciers, already in an ablation-dominated mode, respond immediately to conditions of extremely low snowpack and severe summer drought over the A.D. 1917-1941 interval culminating in retreat rates of >100 m/yr From the mid-1940's to the early 80's retreat rates slowed substantially, with several modest advances documented near the end of the period as the North Pacific transitioned to a cool negative phase resulting in high snow accumulation coupled with mild, intermittent swings between summer drought/pluvial events. Since this time (1980's until ~1998) instrumental records (Figure 3.4*a*) indicate a shift in the aforementioned relationship resulting in continuous, moderate retreat rates.

To illustrate the interaction between proxies, a conceptual mass balance index (MBI) was developed using inferred winter snow accumulation coupled with summer ablation for the past 300 yrs (Figure 3.5). The maximum glacial advance of the LIA coincides with a sustained period of positive MBI that began in the mid-1770's and was interrupted by only one brief ablation phase (~1790's) before the 1830's. The mid 19th century retreat of the Jackson and Agassiz glaciers then coincides with a period marked by strong negative MBI. From this time forward (~1850) Carrara and McGimsey (1981) indicate a modest retreat (<7 m/yr) for both glaciers until approximately 1910, when the MBI shifts to an extreme negative phase.

Conclusions

The evidence presented here suggests that both the late-19th century advance and the rapid early-20th century retreat of GNP glaciers arose from unique (in the context of

these proxy records) interactions between summer ablation and winter accumulation. If couplings of high summer ablation and low winter accumulation become more common under doubled CO_2 conditions, physical and biological systems in the U.S. and Canadian Rockies face widespread and profound changes over the coming decades [*Hall and Fagre*, 2003]. This study also highlights the difficulty in detecting regional impacts of global climate change when decadal-scale climatic variations have a strong influence on local processes.

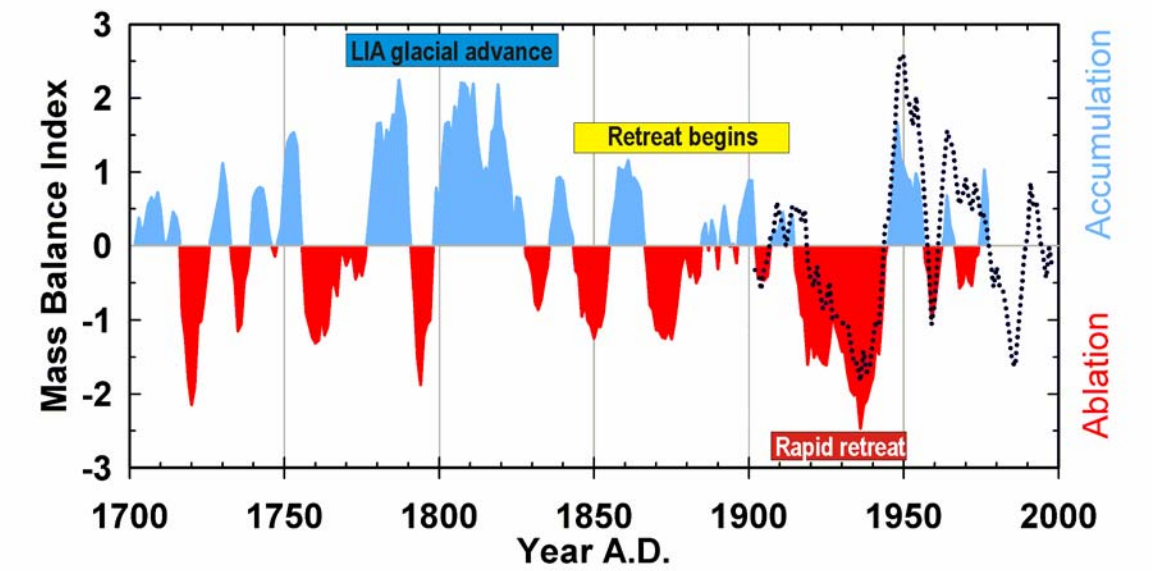

Figure 3.5. By summing the PDO index (Figure 3.4*b*) with the standardized summer drought reconstruction (Figure 3.4*c*) we calculated a proxy index of the drivers of glacial mass balance over the past 300 yrs. The conceptual mass balance index based on proxy data (red and blue fill) is displayed alongside the 20th century index (dotted black line) calculated using instrumental MSD and PDO data.

REFERENCES CITED

Brathwaite, R.J., Olesen, O.B., 1989. Calculation of glacial ablation from air temperature, West Greenland. In: *Glacier fluctuations and climatic change: Proceedings of the symposium on glacier fluctuations and climatic change*, Oerlemans J. [Ed.], Kluwer Academic Publishers, Amsterdam, pp. 219-233.

Biondi, F., Gershunov, A., Cayan, D.R., 2001. North Pacific decadal climate variability since 1661. *Journal of Climate* 16, 5-10.

Bitz, C.M., Battisti, D.S., 1999. Interannual to decadal variability in climate and the glacier mass balance in Washington, Western Canada, and Alaska. *Journal of Climate* 12, 3181-3196.

Carrara, P.E., McGimsey, R.G., 1981. The late neoglacial histories of the Agassiz and Jackson Glaciers, Glacier National Park, Montana. *Arctic and Alpine Research* 13, 183-196.

Carrara, P.E., 1989. Late Quaternary glacial and vegetative history of the Glacier National Park region, Montana, *US Geological Survey Bulletin 1902*.

Cayan, D.R., Dettinger, M.D., Diaz, H.F., Gram, N.E., 1998. Decadal variability of precipitation over western North America. *Journal of Climate* 11, 3148-3166.

Cook, E.R., Kairiukstis, L.A., 1990. *Methods of Dendrochronology: Applications in the Environmental Sciences.* Kluwer Academic Publishers, Boston, 394 p.

D'Arrigo, R.D., Villalba, R., Wiles, G., 2001. Tree-ring estimates of Pacific decadal climate variability. *Climate Dynamics* 18, 219-224.

Hall, M.P., Fagre, D.B., 2003. Modeled climate-induced glacier change in Glacier National Park, 1850-2100. *BioScience* 53(2), 131-140.

Hodge, S.M., Trabant, D.C., Krimmel, R.M., Heinrichs, T.A., March, R.S., Josberger, E.G., 1998. Climate variations and changes in mass of three glaciers in Western North America. *Journal of Climate* 11, 2161-2179.

Luckman, B.H., 2000. The Little Ice Age in the Canadian Rockies. *Geomorphology* 32, 357-384.

Mantua, N., Hare, S., 2002. The Pacific decadal oscillation, *Journal of Oceanography* 58, 35-44.

McCabe, G.J., Fountain, A.G., 1995. Relations between atmospheric circulation and mass balance of South Cascade Glacier, Washington, U.S.A., *Arctic and Alpine Resesearch* 27(3), 226-233.

McCabe, G.J., Dettinger, M.D., 2002. Primary modes and predictability of year-to-year snowpack variations in the western United States from teleconnections with Pacific Ocean climate, *Journal of Hydrometeorology* 3, 13-25.

Newhall, F., Berdanier, C.R., 1996. Calculation of soil moisture regimes from the climatic record. S*oil Survey Investigations Report 46*, USDA Natural Resources Conservation Service, Washington D.C.

Selkowitz, D.J., Fagre, D.B., Reardon, B.A., 2002. Interannual variations in snowpack in the crown of the continent ecosystem. *Hydrological Processes 16*, 3651-3665.

Torrence, C., Compo, G.P., 1998. A practical guide to wavelet analysis. *Bulletin of the American Meteorology Society* 79, 61-78.

CHAPTER 4

THESIS SUMMARY

Summary and Conclusions

Moisture variability is a primary driver of change in physical and environmental systems. It is also of great concern to economists, who use it to make impact assessments of future changes in hydroclimatic variability on local and global economies. However, meteorological data for the northern U.S. Rocky Mountains is limited to the previous 100 years, thus severely restricting the ability to understand long-duration shifts in drought for a region profoundly impacted by decadal-scale precipitation anomalies. The mountainous region encompassed by Glacier National Park, Montana, is an area of high biodiversity and contains a dense concentration of glaciers and perennial snowfields. This makes the hydrological resources in the park and surrounding regions critical for U.S. and Canadian river systems during spring runoff and summer low-flow periods.

Tree rings have been used successfully throughout the western U.S. as proxies for interannual and decadal-scale moisture variability, and often provide records spanning centuries to millennia. Therefore, a summer drought (June-August) reconstruction for the past 461 yrs (A.D. 1540-2000) was developed from a multi-species network of tree-ring chronologies sampled in and around Glacier National Park, Montana. The full drought reconstruction calibrates 44% of the variance (adjusted for degrees of freedom) in the instrumental record, and is based on three of the original eight Douglas-fir (*Pseudotsuga menziesii* (Mirb.) Franco) and limber pine (*Pinus flexilis* James) chronologies. The proxy-

drought reconstruction provides conservative estimates of interannual variation, and tracks low-frequency shifts in the instrumental record well. In addition, the reconstruction bridges the spatial gap between moisture-sensitive reconstructions available for the Canadian Rockies and the central and southern U.S. Rockies, thus allowing for the study of long-term drought variability along a Rocky Mountain transect.

The summer moisture anomaly reconstruction shows that decadal-scale (≥6 yr) deviations from the mean (moisture "regimes") are a common feature throughout the length of the reconstruction. Intervention analysis identifies wet intervals for the region ca. 1572-1578, 1672-1680, 1703-1717, 1770-1791, 1800-1810, 1818-1840, 1899-1916, 1942-1916, 1975-1983, and 1991-1999. The most exceptional period of decadal-scale pluvial events occurs at the height of the Little Ice Age (~ 14th to mid-19th century A.D.) where three long-duration, high-magnitude cool/wet events span approximately 70 yrs combined. No single period over the 20th century was found to contain a decadal-scale pluvial event comparable to that experienced between A.D. 1770-1840. Significant drought regimes are observed between A.D. 1566-1571, 1601-1609, 1626-1641, 1681-1702, 1718-1727, 1754-1769, 1861-1883, 1888-1898, 1917-1941, and 1951-1974. The most extreme of these events was the 1917-1941 event, which spanned more than 25 consecutive years. No other event – drought or pluvial – matches the 1917-1941 drought in duration or magnitude, although the drought event of 1601-1609 and the pluvial event of 1800-1810 exceed the early 20th-century drought event in absolute intensity.

Within a larger context of moisture anomaly reconstructions, located along a north to south transect from the southern U.S. to the northern Canadian Rockies, drought

variability within Glacier National Park appears to be most similar to that experienced in the southeastern Canadian Rockies. Waterton National Park, Alberta, is located to the northeast of Glacier and exhibits moisture anomalies that are tightly coupled with those reconstructed for Glacier. Though the magnitude and intensity of the coincident events may differ, the temporal coherence of the wet and dry moisture anomalies implies that both reconstructions are robust and representative of the region. Along the entire transect, each of the six moisture-sensitive reconstructions exhibits decadal-scale modes of variation in the 20-30 and >50 yr wavelengths, thus suggesting the potential for a common hydroclimatic driver. The network also shows that drought throughout the West operates at continental to regional scales, though the time of onset and intensity between sites may differ. Combining my observations of decadal-scale drought with studies from other researchers, the greatest drought in terms of spatial coherence for the Northern Rockies and the Pacific Northwest appears to be the A.D. 1917-1941 event. As well, the most substantial impacts of this 25-yr drought seem to be centered over northern Washington, Idaho, and Montana.

From the late 19th century to the end of the 20th century, rapid glacial retreat was observed within Glacier National Park. In the simplest form, glacial dynamics are the product of winter accumulation and summer ablation, which are driven by winter snowpack and summer temperatures (i.e. drought) respectively. Within Glacier National Park, winter snowpack levels are tightly linked to sea-surface temperature variations in the north Pacific Basin, which exhibit long-duration shifts in mean temperature. Thus, both summer drought and winter precipitation vary on decadal and multi-decadal

timescales. By using tree-ring based reconstructions of temperature variations in the north Pacific and my drought reconstruction for the Park, I explore the physical drivers of glacial dynamics through long-duration variations in winter accumulation and summer ablation for the past 300 yrs (A.D. 1700-2000).

Results indicate that the Little Ice Age glacial maximum was likely the product of generally high snowpack coupled with cool/wet summers spanning approximately A.D. 1770-1830. Moderate glacial retreat rates coincide with a period of average to below-average snowpack and summer drought that initiates in the mid-1850's and occasionally shifts to mild favorable conditions until A.D. 1917. From the 1920's to the 1940's extreme summer drought coupled with exceedingly low snowpack culminate in glacial retreat rates of >100 m/yr. Thus, the late-19th century glacial advance and early 20th-century rapid retreat appear to be the result of unique decadal-scale pairing of seasonal variations in climate. Also, this research highlights the difficulty in detecting regional impacts of global climate change when 'natural' low-frequency variations in climate exert a strong influence over local ecosystem and physical processes.

Future directions for research related to climate dynamics should seek to address the spatial variability of moisture anomalies throughout the Glacier National Park region. By further expanding the network of moisture-sensitive chronologies throughout the park to include more low-elevation sites, accurate reconstructions of stream flow may become possible for the major hydrological basins. As well, construction of an upper treeline temperature-sensitive network of chronologies would substantially enhance the ability to understand 20th century climate variations and linkages with physical and ecosystem

processes. To this end, this 461 yr reconstruction of summer drought provides an excellent foundation on which to study paleoecological fire events. Collection of mass balance data for a network of the most intensively studied glaciers within the park would also provide an opportunity to more accurately assess the role climate plays in governing glacial dynamics within the park. Furthermore, this would allow for a more precise calibration of my paleo-glacial mass balance model. Finally, the vast network of available hydroclimatic reconstructions for the Canadian and U.S. Rocky mountains should be utilized to further investigate the role of ocean-atmosphere teleconnections in driving the spatial and temporal expression of moisture anomalies evident across the North American Rocky Mountains.

APPENDICES

APPENDIX A

DATA ANALYSIS TECHNIQUES AND CHRONOLOGY CHARACTERISTICS

To develop a better understanding of chronology quality and characteristics, as it relates to species differences and spatial location, each of the 8 chronologies (Figure A.1) in this study were analyzed using the following univariate and multivariate procedures. To begin, as a measure of common signal for each series within a chronology, within-tree, between-tree and mean-tree correlations were calculated over an optimum interval resulting in subsequent average values of r = (0.64), (0.33), and (0.34) (Table A.1). The criterion for selection of optimum interval for each chronology was chosen by ARSTAN and based upon maximization of series length and retention of greatest number of individual series in the data matrix. The between-tree correlations may then be used for an assessment of statistical quality of each chronology as well as increasing error due to decreasing sample depth.

Expressed Population Signal (EPS) provides an overall measure of statistical quality for each chronology based upon between-tree variance and quantifies the degree to which the study chronology represents a hypothetically perfect chronology. EPS as derived by Wigley et al. (1984) is calculated using the equation:

(A.1) $$EPS(t) = \frac{r_{bt}}{r_{bt} + \left(1 - r_{bt}\right)/t},$$

where t is the number of tress averaged and r_{bt} is the mean between-tree correlation. EPS values rise asymptotically from 0 to 1 as number of trees increase to infinity, and there is no suggested maximum or minimum value, although Wigley et at. (1984) consider 0.85 a reasonable value. The signal described by EPS does not necessarily represent climate forcing; other stand-wide factors, such as fire, pests, or pollution, may be represented in

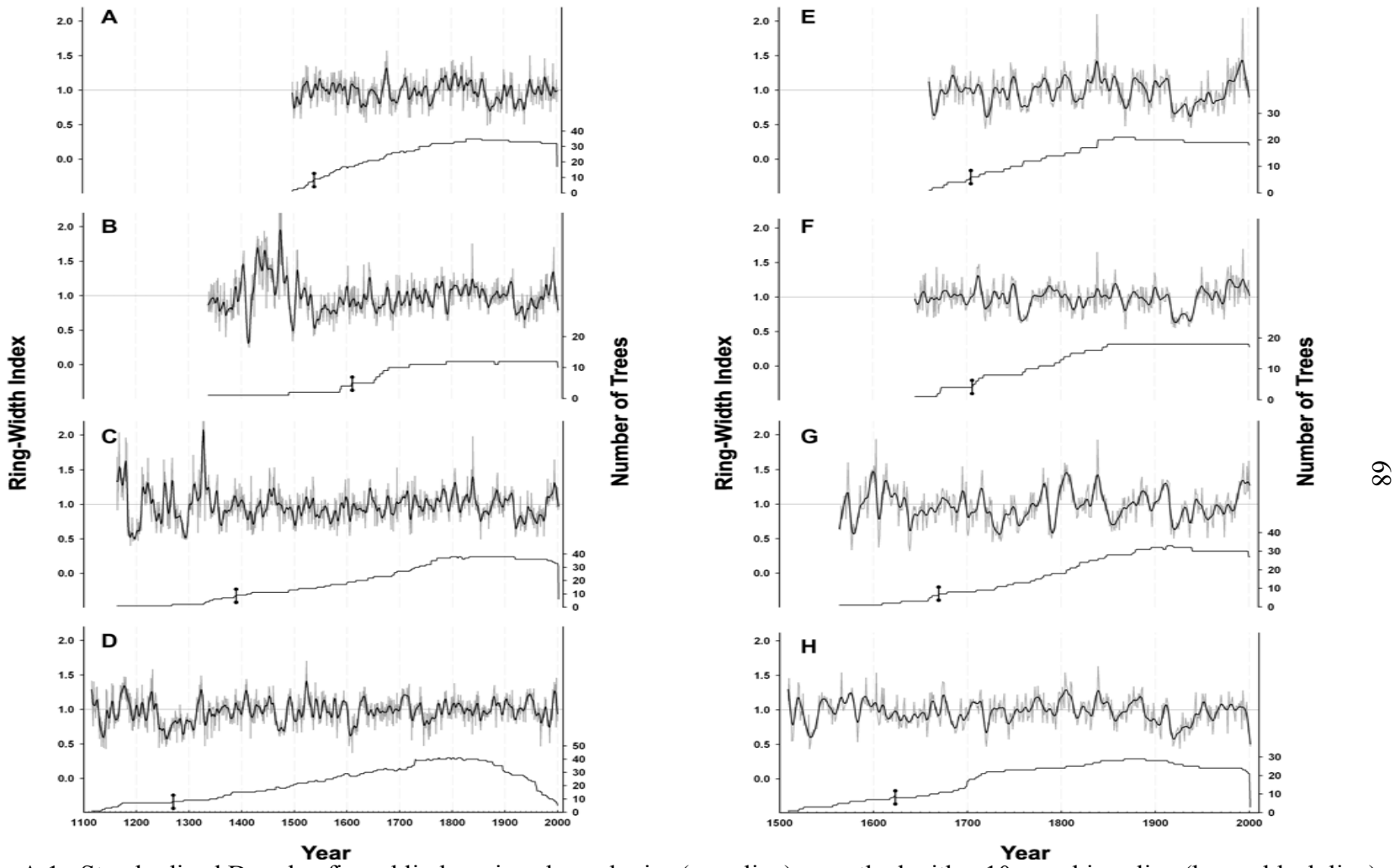

Figure A.1. Standardized Douglas-fir and limber pine chronologies (gray line) smoothed with a 10 yr cubic spline (heavy black line) for; (A) BMS, (B) GTS, (C) SMW, (D) SPW, (E) DOO, (F) NRF, (G) TML, and (H) TRV. Lower line indicates sample depth (number of trees) through time with SSS ≥ 0.85 indicated by a vertical heavy black bar.

Table A.1. Summary statistics for the eight tree-ring chronologies. Light (dark) gray shading indicates chronologies west (east) of the Continental Divide.

Site Code	Mean Series Length (yr)	Mean Sensitivity	Sdev	r_{wt}	r_{bt}	r_{mt}	1st order ACF	EPS ≥ 0.85	SSS ≥ 0.85
BMS	334.0	0.232	0.35	0.62	0.25	0.26	0.38	1618-2001(18)*	1540(9)*
NRF	232.7	0.220	0.32	0.53	0.40	0.40	0.42	1760-2001(9)	1710(6)
DOO	225.4	0.252	0.50	0.78	0.40	0.41	0.53	1740-2001(9)	1704(6)
GTS	330.0	0.214	0.23	0.60	0.33	0.34	0.64	1790-2000(12)	1610(5)
TML	219.9	0.248	0.52	0.64	0.38	0.38	0.61	1730-2001(10)	1670(7)
SMW	376.2	0.235	0.29	0.69	0.33	0.33	0.58	1489-2001 (12)	1386(8)
TRV	261.5	0.242	0.35	0.69	0.28	0.29	0.53	1700-2000(15)	1618(8)
SPW	341.2	0.236	0.22	0.59	0.29	0.30	0.50	1380-1970 (14)	1268(8)
Mean	290.1	0.235	0.35	0.64	0.33	0.34	0.52		

Note: All statistics are derived using an optimal interval based on sample size and depth for each chronology. Mean sensitivity (Fritts, 1976) and standard deviation (Sdev) provide estimates of inter-ring variability and overall chronology variability respectively. r_{wt}, r_{bt} and r_{mt} are the within-tree, between-tree, and mean correlations used for calculation of EPS and SSS. The express population signal (EPS) is a measure of chronology statistical quality, and subsample signal strength (SSS) provides an estimate of increasing chronology error due to decreasing sample size (Wigley et al., 1984; Briffa and Jones, 1990). First order ACF is the lag 1 serial correlation coefficient for each chronology.

* Number of trees

this value. The range of years and number of trees required for each chronology to attain and EPS value ≥ 0.85 are presented in table A.1.

EPS does not represent the most relevant statistic of chronology error as it relates to decreasing sample depth through time. To constrain additional error in climate reconstructions resulting from decreasing sample depth in the early portion of the record, Subsample Signal Strength (SSS) was computed for each chronology (Wigley et al., 1984). SSS provides an estimate of how well a reduced number of series represents the full chronology - or population of trees sampled. SSS as derived by Wigley et al. (1984) is calculated using the equation:

$$SSS = \frac{t'\left[1 + (t-1)r_{bt}\right]}{t\left[1 + (t'-1)r_{bt}\right]}, \tag{A.2}$$

Where t is the total number of trees in the sample and t' is the tree number in the subsample, while r_{bt} represents the mean between-tree correlation. An SSS value of 0.85 was selected as the cutoff, thus limiting the maximum amount of additional error arising from a decreasing number of trees at 15%. Due to larger between-tree variation at each site, an SSS value of 0.85 was attained with seven trees on average, which is slightly higher than other western conifer chronologies, probably resulting from any number of local factors. SSS dates and tree numbers are plotted in figure A.1 and can be located in table A.1 along with other additional general chronology statistics.

For an assessment of site similarity correlation analysis and factor analysis methods were utilized. A common interval for investigation of chronology interrelatedness was established using the SSS cutoff value of the shortest chronology (NRF) resulting in a truncation date for all chronologies at A.D. 1710. Initial relationships between chronologies were established by means of Pearson-product moment coefficients. For investigation of latent relationships between chronologies as it relates to spatial gradients or species differences, principal components factor analysis was employed. The goal of factor analysis is to explain associations between variables through a smaller number of indices or factors. These analyses were carried out on the standardized correlation matrix of all chronologies. The assumption of multivariate normality was met by investigating univariate normality using histograms and normal quantile distribution plots. A subjective step in factor analysis is selection of m, the number of common factors to which the complete set of variables will be reduced. Here, m was selected based upon the number of potential groupings evident in the correlation

matrix (Table A.2), and the proportion of variance explained by each of the eigenvalues. Two final values for *m* were selected (*m* = 3; *m* = 4) as a test in the robustness of the potential structure as it relates to spatial distribution and species differences. The total percentage of variance explained by using *m* = 3 and *m* = 4 is 80.4% and 87.3% respectively, indicating both models are able to capture and explain the majority of the variability between chronologies. Finally, to aid in interpretation of the factor loadings a varimax rotation was performed.

Table A.2. Between-site correlations for all chronologies over common period 1710-2000. Light (dark) gray shading indicates Douglas-fir chronologies west (east) of the divide. Dark blue shading indicates correlation values between sites located on opposing sides of the Continental Divide. The limber pine chronology is located at the bottom of the table and highlighted in light blue.

Site Code	BMS	NRF	DOO	GTS	TML	SMW	TRV
NRF	0.709						
DOO	0.627	0.771					
GTS	0.573	0.582	0.759				
TML	0.428	0.416	0.602	0.626			
SMW	0.554	0.602	0.757	0.769	0.707		
TRV	0.382	0.413	0.511	0.54	0.458	0.606	
SPW	0.309	0.367	0.329	0.262	0.365	0.368	0.211

Between-site correlations for all Douglas-fir chronologies range from 0.382 to 0.771, suggesting a combination of local- and regional-scale factors affecting tree growth (Table A.2). The overall mean correlation between all sites is $r = 0.522$ (p-value < 0.000), with Douglas-fir sites having $r = 0.590$ (p-value < 0.000). This indicates a moderately high degree of similarity in low- and high-frequency variation. The relationships improve when correlations between Douglas-fir sites located west of the CD ($r = 0.702$ [p-value <0.000]) and east of the Continental Divide ($r = 0.618$ [p-value <

0.000]) are analyzed separately. These results could indicate a common growth forcing related to climate factors (specific to position in relation to the Continental Divide).

Using results obtained when the number of common variables (*m*) is reduced to 3 we find factor 1 loads strongly on the four Douglas-fir chronologies east of the Divide, explaining 35.3% of the total variance (Table A.3). Conversely, factor 2 groups the three Douglas-fir chronologies west of the Divide explaining a total of 31.1% of the variance. A potential reason for such clustering may be related to differences in evapotranspiration rates on the eastern and western sides of the Continental Divide, thereby providing a similar and constant forcing within each group. Finally, the single limber pine chronology is the sole significant loading on factor 3, explaining an additional 14% of the total variance. This may be representative of a different species-specific response to drought related to how drought stress is incorporated into growth.

Table A.3. Rotated factor loadings and communalities for all chronologies computed using the principal component method and $m = 3$.

Variable	Factor1	Factor2	Factor3	Communality[a]	Specific[b] Variances
SMW	0.785	0.427	0.198	0.837	0.163
TML	0.778	0.177	0.321	0.740	0.260
TRV	0.778	0.183	-0.014	0.638	0.362
GTS	0.723	0.503	0.045	0.778	0.222
NRF	0.262	0.871	0.179	0.860	0.140
BMS	0.235	0.847	0.129	0.789	0.211
DOO	0.576	0.691	0.125	0.825	0.175
SPW	0.144	0.187	0.954	0.966	0.034
Proportion of Total Variance	0.353	0.311	0.140	0.804	

[a] Proportion of variance contributed by *m* common factors.
[b] Uniqueness or proportion of variance contributed by the specific factor.

By increasing *m* to four common variables, similar results are obtained. However, some interesting differences emerge. Table A.4 indicates that western and eastern chronologies still cluster, with western chronologies loading on factor 1 and eastern on factor 2. Both of the eastern and western clusters explain approximately equal proportions of the variation (30.4% vs. 29.1% respectively), and the SPW limber pine chronology displays its uniqueness from the Douglas-fir chronologies by loading on the final factor. However, the TRV chronology no longer clusters with the other eastern chronologies, and can be found as the sole significant loading on factor 3. The removal of TRV from a clustering with other eastern chronologies may indicate TRV is located in a region influenced by a different climate or is possibly the result of unique local site characteristics.

Table A.4. Rotated factor loadings and communalities for all chronologies computed using the principal component method and $m = 4$.

Variable	Factor1	Factor2	Factor3	Factor4	Communality[a]	Specific[b] Variances
NRF	0.871	0.224	0.163	0.182	0.868	0.132
BMS	0.844	0.220	0.119	0.125	0.790	0.210
DOO	0.677	0.566	0.220	0.085	0.834	0.166
TML	0.144	0.883	0.129	0.223	0.867	0.133
SMW	0.411	0.722	0.358	0.154	0.843	0.157
GTS	0.485	0.703	0.274	-0.010	0.804	0.196
TRV	0.210	0.290	0.925	0.072	0.988	0.012
SPW	0.184	0.170	0.066	0.959	0.987	0.013
Proportion of Total Variance	0.304	0.291	0.146	0.132	0.873	

[a] Proportion of variance contributed by *m* common factors.
[b] Uniqueness or proportion of variance contributed by the specific factor.

Observation of relationships between chronologies using factor-loading plots yields conclusions identical to those obtained through interpretation of sorted factor loadings. Figure A.2 displays the clustering of chronologies located east and west of the Continental Divide (for m = 3 and m = 4), as well as the uniqueness of TRV and SPW. Of further interest are the two chronologies - DOO and GTS - that could arguably be placed with either the eastern or western chronologies due to their rotated factor loadings (Table A.3; A.4), as well as their location in the factor loading plots (Figure A.2). In figure A.2 it appears that GTS groups with a cluster containing other eastern chronologies, but DOO has no obvious association with either the eastern or western chronology grouping. A potential explanation for such a response may be the result of the position of DOO in the southwest corner of the park, west of the CD and directly west of the majority of the eastern chronologies. Without better spatial replication of Douglas-fir chronologies it is hard to accurately assess the exact spatial relationships, but it does appear that a strong west to east gradient exists, with the potential for differences arising along a north to south distribution.

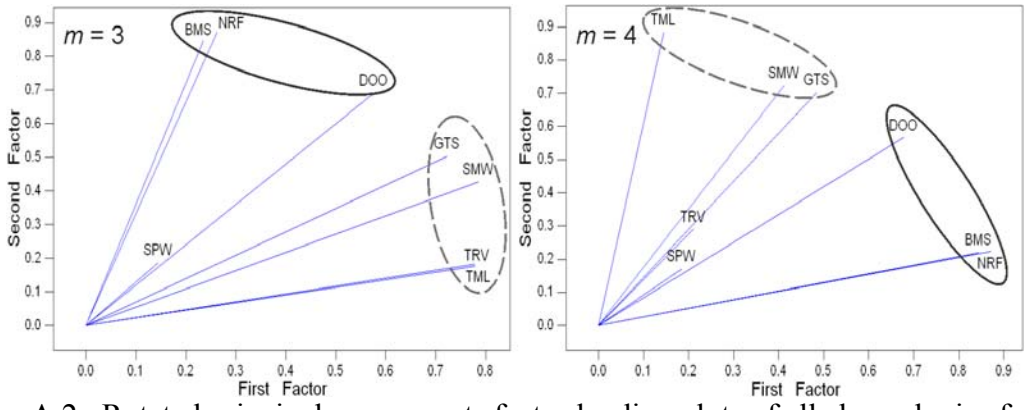

Figure A.2. Rotated principal components factor loading plots of all chronologies for $m = 3$ and $m = 4$ common factors. Douglas-fir chronologies located west (east) of the Continental Divide are circled with a solid (dashed) black line.

APPENDIX B

CLIMATE DATA ACQUISITION

Historical weather data was obtained from the Western Regional Climate Center (WRCC; http://www.wrcc.dri.edu/) and the U.S. Historical Climatology Network (USHCN; http://cdiac.esd.ornl.gov/epubs/ndp019/ndp019.html). Both data repositories provide monthly historical weather data, but the USHCN provides adjustments to temperature records for station moves, introduced time of observation biases, and interpolated values for missing precipitation and temperature records to 1994 (Easterling et al., 1996). The WRCC provides the original station data for monthly maximum, minimum, and average temperature, total precipitation, and metadata related to missing values from the beginning of the record to present. For inclusion in the USHCN, a station must have a long period of record (>80 yrs), be relatively serially complete, and have a low probability for introduction of bias caused by meteorological station moves. The Kalispell WSO AP and Fortine 1N station record meet all of the above criteria, but Kalispell was subject to fewer station moves, spans a longer period of time, and is missing the least amount of data. Therefore Kalispell was selected as the primary station for use in analysis of climate-growth relationships.

There are, however, some important differences between the USHCN and the WRCC weather data. For instance, corrections made to the minimum temperature record by the USHCN offset the average summer minimum temperatures at the beginning of the century by ~2°C when compared with the raw WRCC summer minimum temperatures (Figure B.1*a*). This results in a positive trend in the USHCN summer minimum temperatures not evident in the WRCC raw data. However, adjustments made to the USHCN record coincide with the recorded station moves of 1949 and 1959, and exhibit

general agreement with the positive summer minimum temperature trend found in the nearby Fortine 1N WRCC and USHCN records (Figure B.1*b*). This change in the record has little to no impact on results obtained from analysis of climate-growth relationships, but it does have potential implications for the Palmer Drought Severity Index (PDSI) and mean summer deficit (MSD) drought index calculated for the Kalispell meterological station. This occurs due to the utilization of temperature as a key climate parameter from a station's historical data for construction of both PDSI and MSD. In general, any study that makes use of minimum and average historical temperature records for the Kalispell WSO AP station should take into account both the raw WRCC or adjusted USHCN record. For this study, the adjustments made to the Kalispell temperature records are robust and justifiable, however corrections made to precipitation records for stations located in regions of high topographic relief can be tenuous and should be evaluated on a station-by-station basis.

Several changes made by the USHCN to the Kalispell precipitation record influenced my decision to use the raw WRCC Kalispell precipitation data. First, the USHCN data reports missing values for August in years 1978-1982 that are present with no missing values in the WRCC record (Figure B.1*c*). As well, there are inconsistencies in adjustments made to precipitation values in the early portion of the record (1900-1905), where no station moves are indicated, and missing values do not present a problem. Many of the interpolated monthly values were flagged by USHCN as having poor confidence intervals around the estimated values or were replaced with values interpolated from another regional station. For these reasons, and because a complete

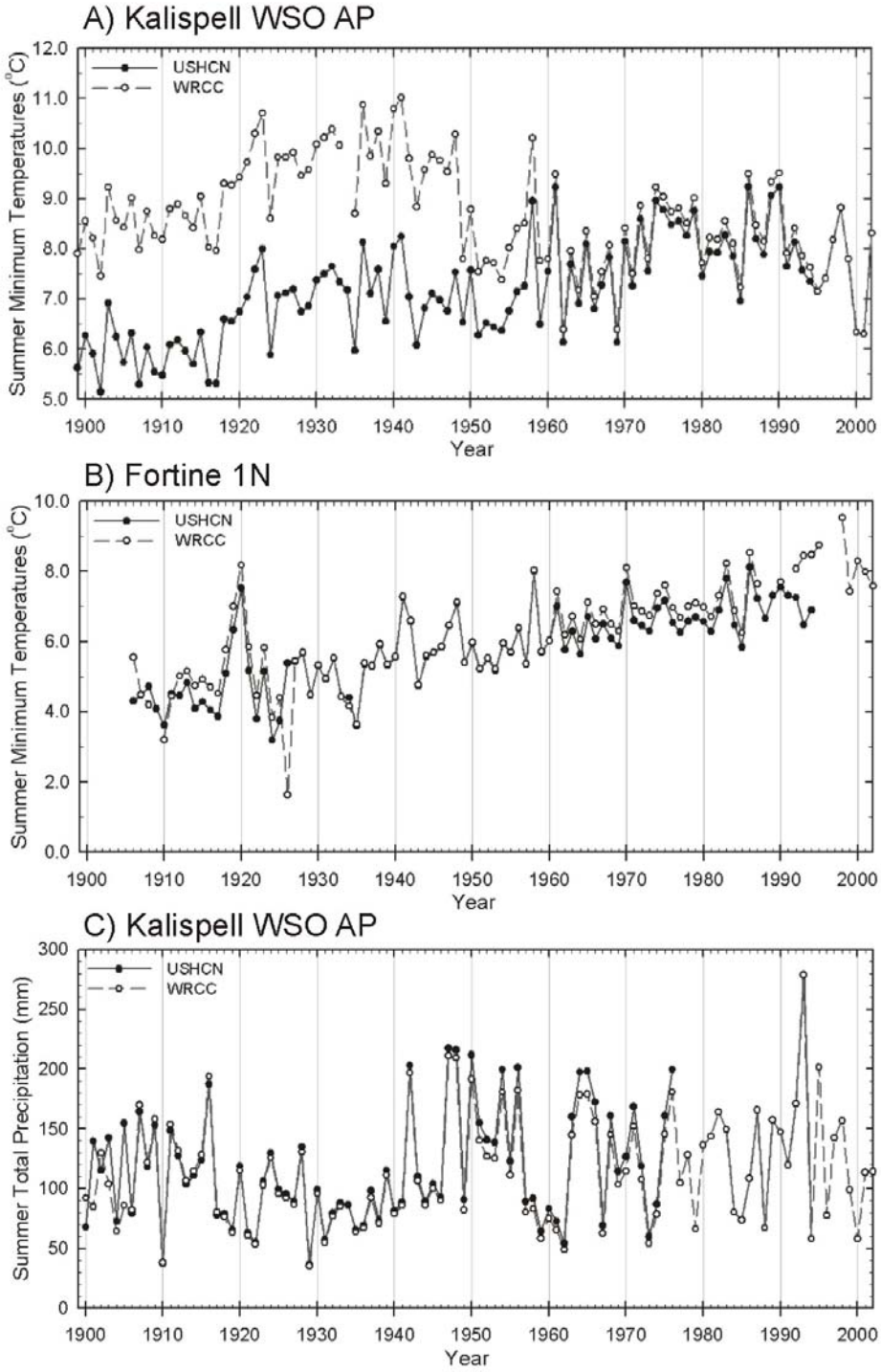

Figure B.1. Comparison of USHCN and WRCC summer minimum temperature data for Kalispell WSO AP (A), and Fortine 1N (B) meteorological stations. As well, USHCN and WRCC comparisons are made for total summer precipitation data recorded by the Kalispell WSO AP (C) station.

record is available to 2003, the WRCC precipitation data was selected for use in the final drought models along with the USHCN average temperature records. The combination of these two records results in missing data only for 1949 when the station was moved and no records were kept from January to May. By combining the WRCC and the USHCN record, we ensure the use of a temperature record unbiased by station moves, heat island effects, and observation times along with the most serially complete record of precipitation data.

APPENDIX C

CALCULATION OF DROUGHT SEVERITY INDICES

Calculation of MSD (Precipitation – Potential Evapotranspiration for JJA) and PDSI was performed using the Newhall Soil Moisture and PDSI software available from the National Agriculture Decision Support System (http://nadss.unl.edu/index.php). This MSD water balance model is parameterized using the latitude, longitude, hemisphere, and soil parameters related to temperature and pore geometry of a meteorological station. The input data used to calculate MSD are monthly total precipitation and monthly average temperature. Average temperature - in conjunction with day length - is used to estimate potential evapotranspiration (PET), which is calculated using a procedure outlined in Thornthwaite (1948). Figure C.1 shows a water-balance model for the Kalispell weather station that may be considered representative of the GNP region. The general regional pattern is as follows: soil moisture recharge from winter precipitation; spring melt resulting in the majority of the winter precipitation leaving the system through leaching and runoff; and a summer moisture deficit resulting from a large increase in PET and absence of ample rainfall.

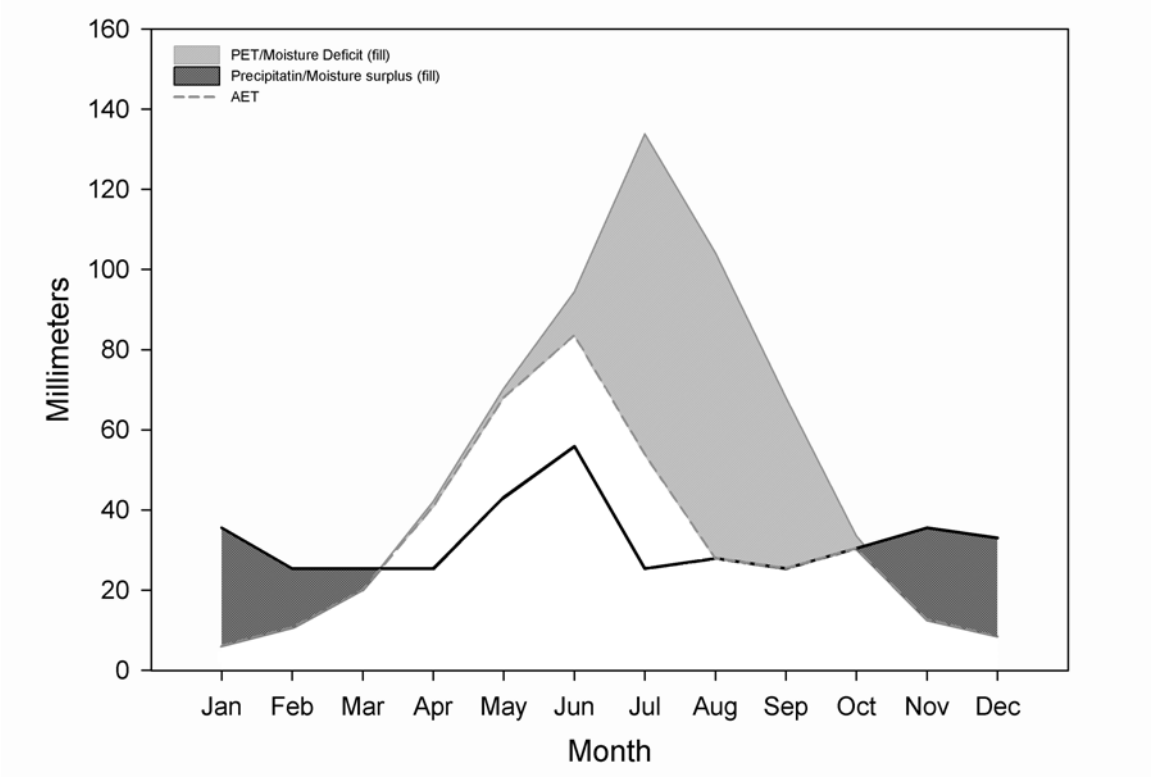

Figure C.1. Water-balance diagram for Kalispell, Montana. Average monthly total precipitation (thick black line), actual evapotranspiration (AET; dashed gray line), and potential evapotranspiration (PET; solid gray line) are plotted for each month. The light gray fill represents summer moisture deficit, or MSD, and the winter/spring moisture surplus is shaded dark gray.

APPENDIX D

DATA CALIBRATION AND MOVING CORRELATION COEFFICIENTS

Calibration of the tree-ring and climate data was conducted using correlation analysis over a 15-month period spanning the previous June to August of the growth year for each of the 8 chronologies. Relationship to total precipitation (PPT), maximum temperatures (T_{max}), average temperatures (T_{avg}), and minimum temperatures (T_{min}) were investigated on a monthly, seasonal, and annual basis from 1900-2001. To reduce the probability of identification of spurious relationships the data was bootstrapped 1000 times over the entire 102 yr period and only values exceeding the 95% significance level are presented (results are reported and discussed in depth in Chapter 2).

For an assessment of temporal stability of the climate-tree growth relationship, moving (MCC) and evolutionary correlation coefficients (ECC) were calculated utilizing DendroClim2002 software (Biondi, 1997). As described by Biondi (1997, 2000), MCC's are calculated by sliding a "window" of a set number of years across the time series in annual increments. ECC's work by progressively changing the period of years used in calibration, thus analysis may proceed forward or backward through selection of a fixed start year at the beginning or end year of a record, respectively. Interpretation of results obtained from both MCC and ECC analysis can provide information on subtle changes in climate/tree-growth relationships, but MCC's produce more robust information because statistical significance is assessed using a constant sample size (Biondi, 2000). Consequently, only findings from MCC analysis will be presented here. To maintain a sufficient number of degrees of freedom for significance testing, only periods ≥ 35 yrs. were considered. In both MCC and ECC analysis, significance is assessed at the 95% confidence level by bootstrapping the data 1000 times with each forward step of the

MCC or widening of the ECC. Results are presented in pseudo-color plots (or contour plots) with the correlation coefficient represented in color on the z-axis and arbitrarily plotted as the last year of the 35 yr window on the x-axis. The month or season associated with the correlation coefficient value is labeled and plotted on the y-axis.

By utilizing short (35 yr) MCC's I was able to ascertain how the climate/growth signal has changed through time as well as potential "windows" in time with complete absence of significant relationships. Figure D.1 shows monthly T_{max} and PPT correlations for the 3 western Douglas-fir chronologies (BMS, NRF, DOO) and the single eastern limber pine chronology (SPW). The limber pine chronology (Figure D.1 *bottom*) exhibits overall weak correlation with a sporadic temporal signal to both T_{max} and PPT over the entire length of record. SPW may, however, provide a more robust seasonal signal and capture a component of climatic information not present in the Douglas-fir chronologies when used in a multi-species reconstruction of drought. Therefore the chronology was retained for further analysis. The three Douglas-fir chronologies (BMS, NRF, DOO) exhibit consistently strong negative correlation to previous July T_{max}. June T_{max} displays a strong relationship with ring-width variability over the first half of the century; however, the association shifts to August T_{max} during the latter half of the 20^{th} century. Each of the Douglas-fir chronologies in figure D.1 also indicate a high correlation with spring-summer T_{max} of the growth year during the first half of the century coinciding with a severe 25-year drought (1917-1941). This relationship may be representative of a non-linear response in tree-growth during severe drought, wherein the response of a tree to temperature (i.e. moisture stress) during the growth year becomes

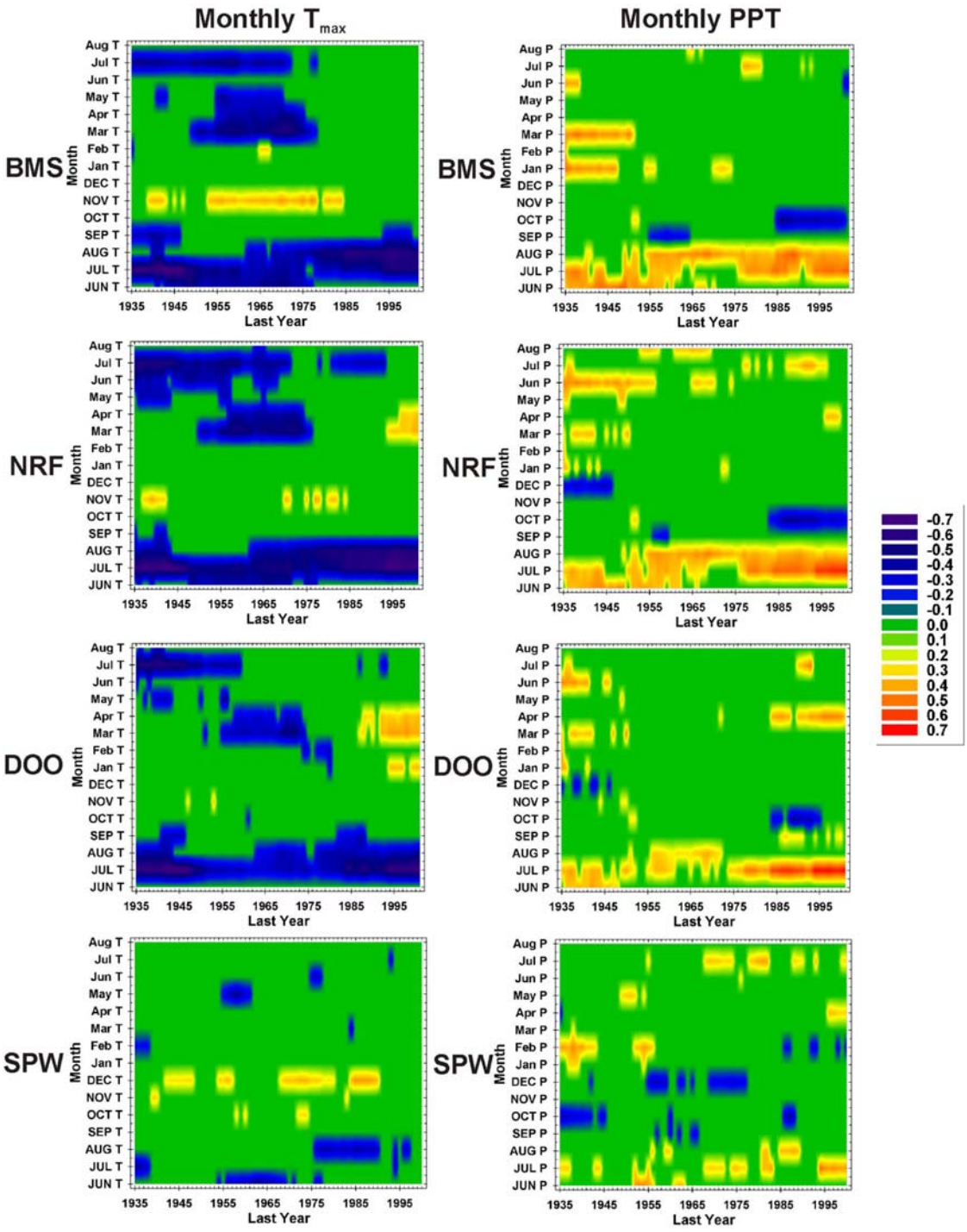

Figure D.1. Thirty-five year monthly MCC's for three Douglas-fir ring-width chronologies located west of the Divide, and the single limber pine chronology. Months are ordered from bottom to top starting with June (JUN) of the previous year to August (Aug) of the growth year. The correlation coefficient value is plotted at the last year of the 35 yr moving window. Only values exceeding the 95% confidence level are shown.

more critical in determining growth for that year. In contrast, the high correlations are undoubtedly related to the high degree of interannual temporal autocorrelation present during prolonged periods of severe drought.

The same patterns described for monthly temperature are present in monthly relationships to PPT for the 3 Douglas-fir chronologies. During the first half of the 20th century, previous year June-July PPT correlate strongest with ring-width, shifting around 1950 to correlating strongly with July-August PPT. Each of the chronologies also exhibits a weakening of correlation coefficient values and the temporal stability of the PPT signal when compared with T_{max}. Correlation between ring-width and PPT during the winter and spring months of the current year are sporadic, but also indicate that these months may become more important for initiation of cambial activity during severe drought.

For the Douglas-fir chronologies east of the CD (GTS, TML, SMW, TRV), the patterns of the T_{max} and PPT relationships are similar with the exception of reduced temporal stability of the PPT signal in all chronologies, as well as with the T_{max} signal in TML and TRV (Figure D.2). This overall reduction in temporal stability of signal and correlation coefficient strength may be in large part related to climatic differences experienced east of the CD and the inability of the Kalispell weather station record to be completely representative of that climate. One striking difference in the eastern Douglas-fir chronologies is that TRV and SMW have some of the strongest correlations of any chronologies used in this study to T_{max} of the current growth year. As well, TRV exhibits remarkable temporal stability with current year January and June PPT, which is not

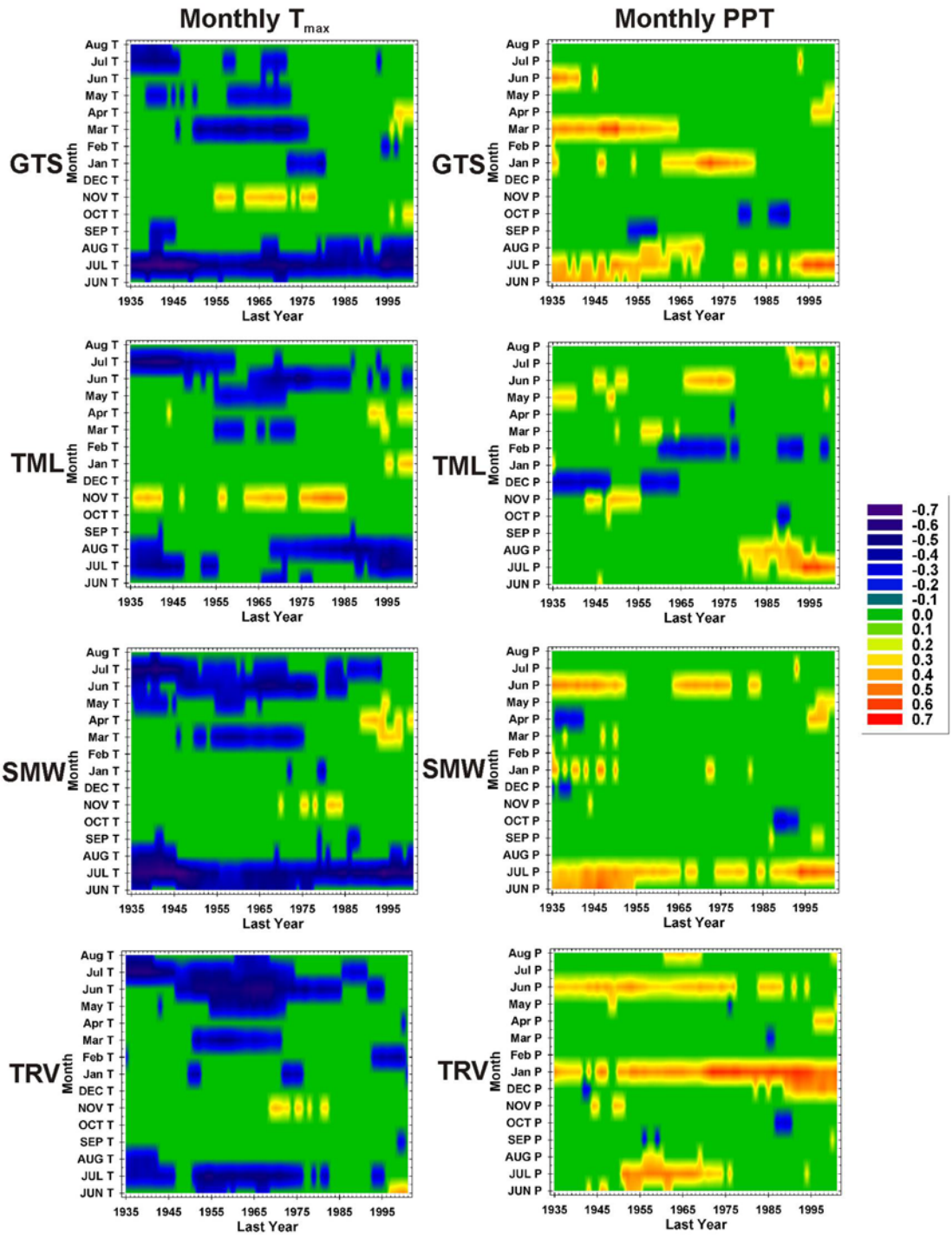

Figure D.2. Thirty-five year monthly MCC's for the four Douglas-fir ring-width chronologies located east of the Divide. Months are ordered from bottom to top starting with June (JUN) of the previous year to August (Aug) of the growth year. The correlation coefficient value is plotted at the last year of the 35 yr moving window. Only values exceeding the 95% confidence level are shown.

apparent in any other records. Coinciding with results from factor analysis, TRV may represent a change in Douglas-fir physiological response to climate, or the chronology may be located in a different climatic region from GNP.

The structure of monthly climate/ring-width correlations indicates a strong response to current and previous summer T_{max} and PPT. Results obtained from seasonal averages of T_{max} and PPT indicate an overall increase in the strength of the relationship. The 35 yr seasonal MCC's for each chronology exhibited in figure D.3 demonstrate that the overall temporal stability of the signal is improved for summer (T_{max}, PPT) and current winter (January-April) total precipitation. The signal is inconsistent in TRV, SPW and TML, but the seasonal averages do represent an overall improvement over monthly relationships. One final caveat should be noted: the use and of 35 yr MCC's requires caution during interpretation. Due to the short length of the window, correlation coefficients may be heavily influenced by the presence of several outliers, even when bootstrapped 1000 times. Lengthening the window prevents extreme positive or negative correlations, thereby reducing the influence of outliers and consequently circumventing the problems encountered from using short windows.

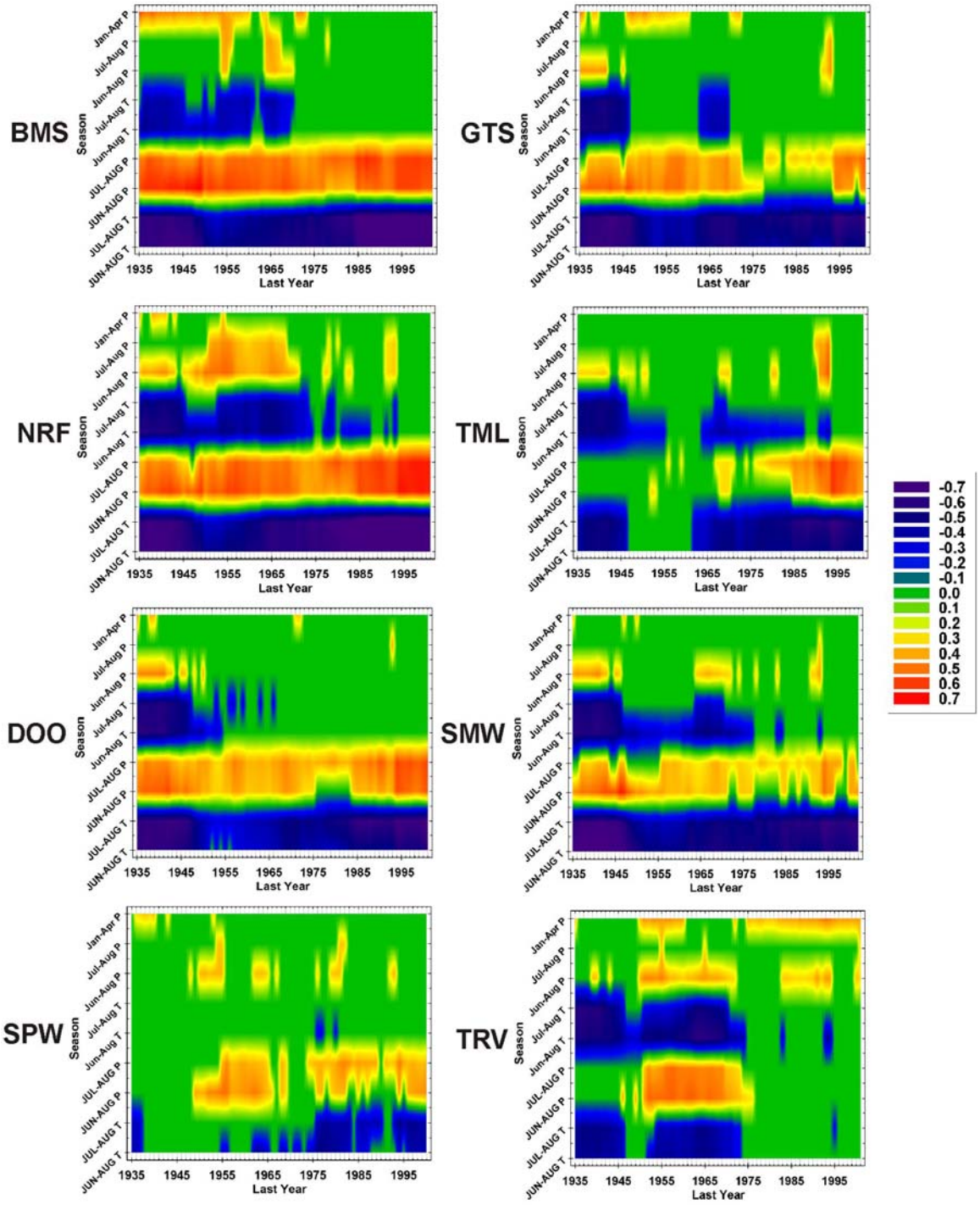

Figure D.3. Thirty-five year seasonal MCC's for all eight chronologies. Seasons are ordered from bottom to top starting with Summer T_{max} (JUN-AUG T) of the previous year to Winter-Spring PPT (Jan-Apr P) of the growth year. The correlation coefficient value is plotted at the last year of the 35 yr moving window. Only values exceeding the 95% confidence level are shown.

APPENDIX E

FREQUENCY CHARACTERISTICS OF DROUGHT RECONSTRUCTIONS ALONG A NORTH TO SOUTH ROCKY MOUNTAIN TRANSECT

Here I present the frequency characteristics of moisture anomalies along a north to south transect spanning the U.S. and Canadian Rockies. Signals are isolated using the multi-taper spectral analysis method (MTM), whereby the background noise (red noise) is estimated using a 'robust' procedure that is largely unbiased by climatic signals immersed in noise (Mann and Lees, 1996). This method provides a distinction between purely harmonic and broader band signals contained within a time series, thus increasing the overall effectiveness of the procedure in detecting actual signals rather than artifacts arising from noise present in the time series (*see* Mann and Lees, 1996).

For each of the moisture anomaly reconstructions, MTM analysis was conducted over a common interval (A.D. 1540-end of record) even though many of the reconstructions extend back further through time. This is due to inconsistency of decadal-scale variations in precipitation throughout the length of climatic time series. Subsequently, all of the reconstructions exhibit significant (≥95% CI) modes of variation in the decadal (20-30 yr) and multidecadal (≥50 yr) wavelengths (Figure E.1, E.2, E.3, E.4, E.5, E.6). Waterton NP, however, is an exception in that it's missing a significant frequency spike in the 20-30yr bandwidths, which is most likely due to the short duration of the record (A.D. 1710-1996; Figure E.2). The Uinta Basin, Utah, also exhibits slightly lower-frequency variation at decadal scales, showing a significant peak in the 39-46 yr frequency range (Figure E.5). Although the frequency spikes within the decadal-scale range of variability are slightly different, each of the moisture anomaly reconstructions were smoothed with a 25yr spline to highlight similarities and differences in this low-frequency range of variation.

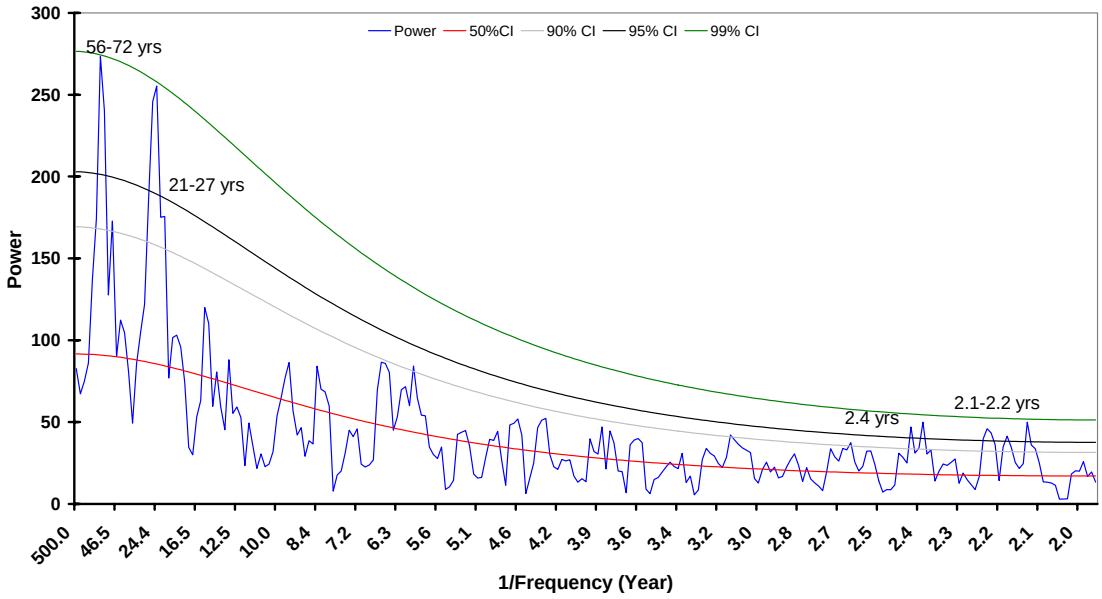

Figure E.1. MTM spectrum (blue line) of the Banff NP annual precipitation reconstruction showing confidence intervals (CI) at the 50% (red line), 90% (gray line), 95% (black line), and 99% (green line) levels. The spectrum is constructed using a robust red noise background (AR 1) over the A.D. 1540-1994 interval.

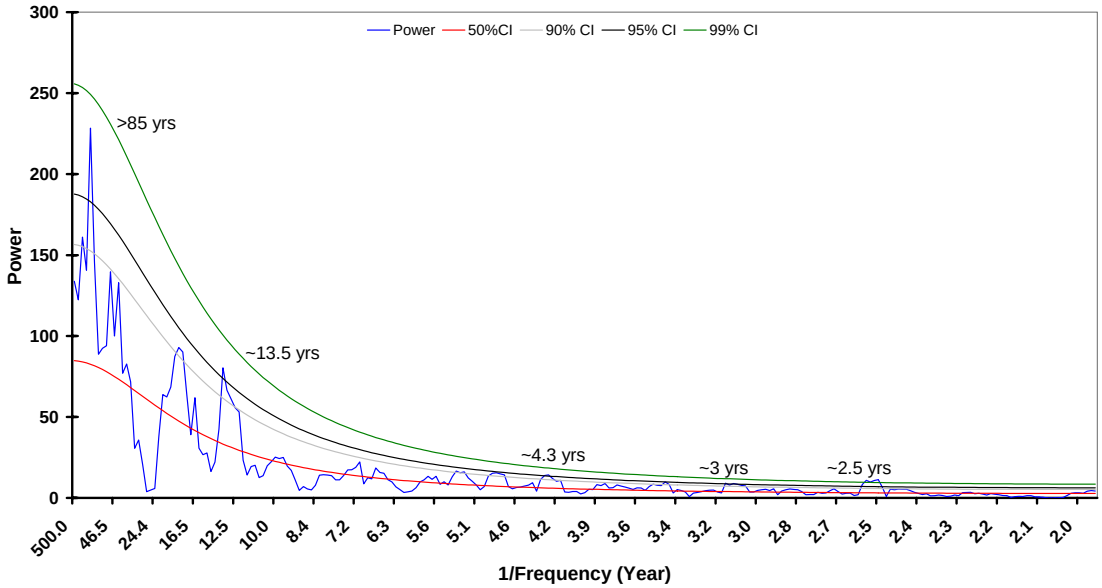

Figure E.2. MTM spectrum (blue line) of the Waterton NP annual precipitation reconstruction showing confidence intervals (CI) at the 50% (red line), 90% (gray line), 95% (black line), and 99% (green line) levels. The spectrum is constructed using a robust red noise background (AR 1) over the A.D. 1710-1996 interval.

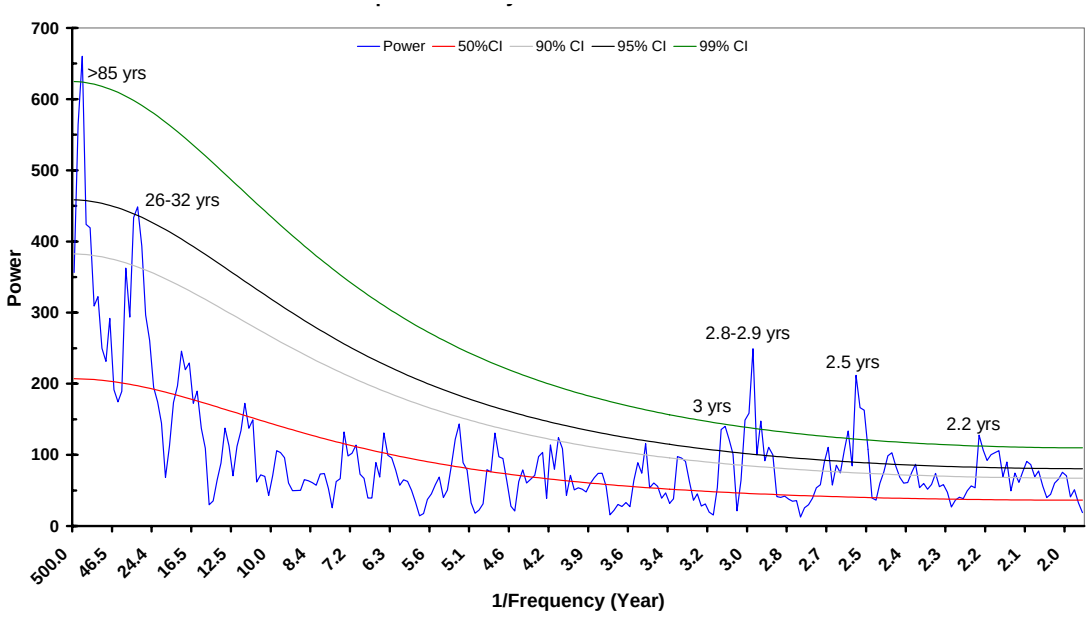

Figure E.3. MTM spectrum (blue line) of the Glacier NP summer drought reconstruction showing confidence intervals (CI) at the 50% (red line), 90% (gray line), 95% (black line), and 99% (green line) levels. The spectrum is constructed using a robust red noise background (AR 1) over the A.D. 1540-2000 interval.

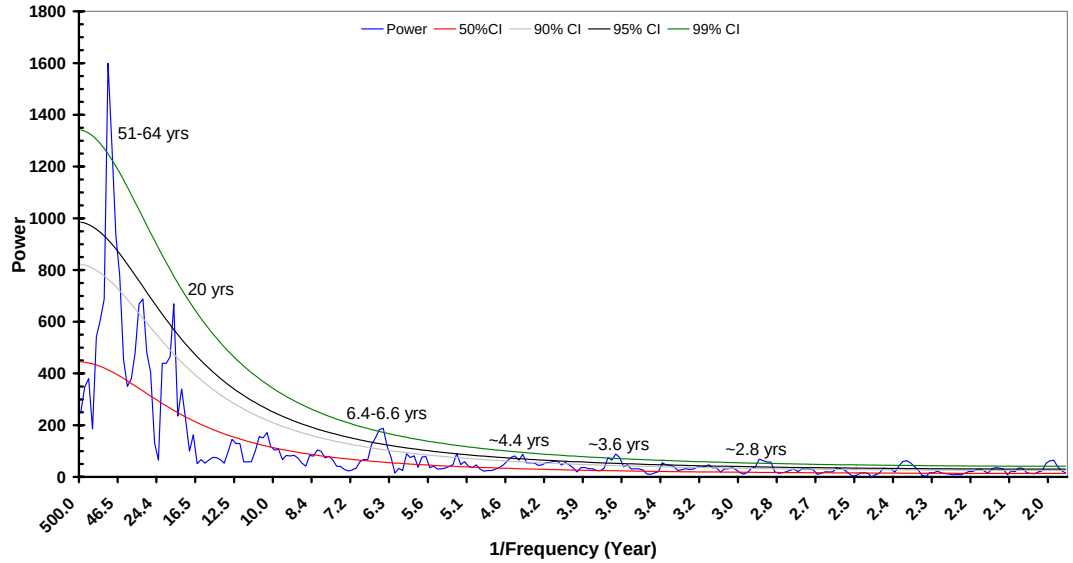

Figure E.4. MTM spectrum (blue line) of the Yellowstone NP annual precipitation reconstruction showing confidence intervals (CI) at the 50% (red line), 90% (gray line), 95% (black line), and 99% (green line) levels. The spectrum is constructed using a robust red noise background (AR 1) over the A.D. 1540-1997 interval.

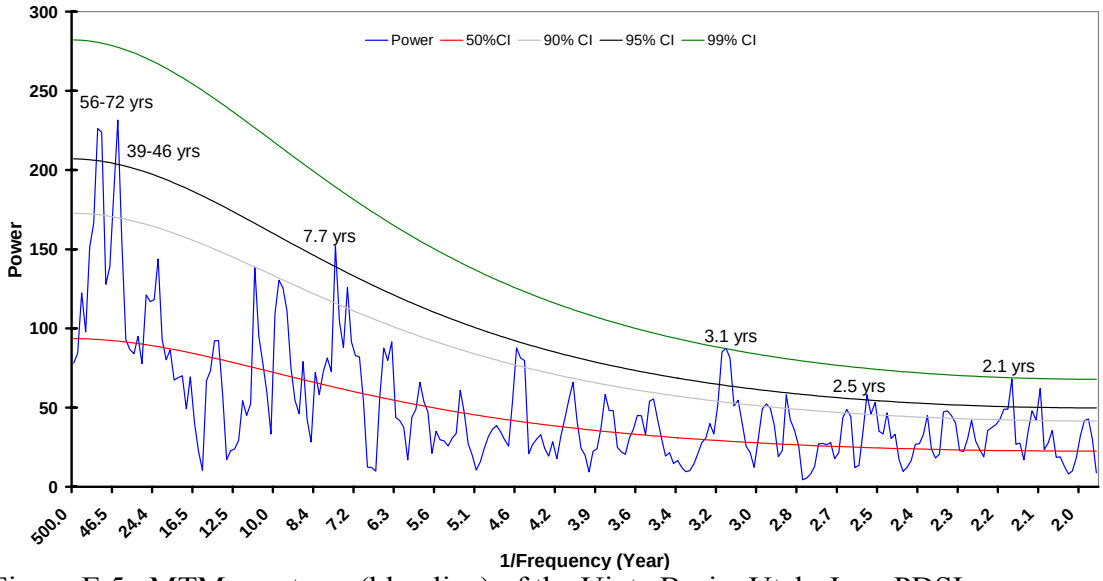

Figure E.5. MTM spectrum (blue line) of the Uinta Basin, Utah, June PDSI reconstruction showing confidence intervals (CI) at the 50% (red line), 90% (gray line), 95% (black line), and 99% (green line) levels. The spectrum is constructed using a robust red noise background (AR 1) over the A.D. 1540-2000 interval.

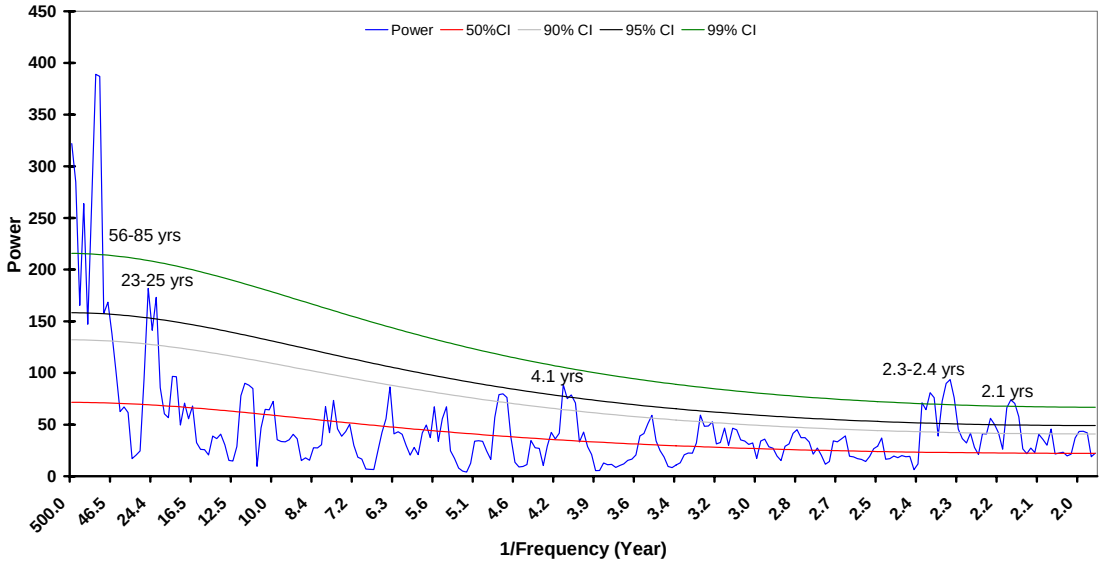

Figure E.6. MTM spectrum (blue line) of the El Malpais NM, annual precipitation reconstruction showing confidence intervals (CI) at the 50% (red line), 90% (gray line), 95% (black line), and 99% (green line) levels. The spectrum is constructed using a robust red noise background (AR 1) over the A.D. 1540-1992 interval.